CHAPTER 6

ANALYSIS OF THE ISOLATED SUBHARMONIC SOLUTIONS – PRACTICAL CASE STUDIES

6.1 INTRODUCTION

This chapter is concerned with the analysis of isolated subharmonic ferroresonant solutions in practical systems. As mentioned in Chapter 5, the isolated subharmonic solutions are detected by temporal bifurcation diagrams. Two reported cases of ferroresonance involving the network of Bonneville Power Administration (BPA), U.S.A., are considered for analysis. The system corresponding to the first case is same as the one described in Chapter 3. The second case involves the 525 kV transmission system of BPA between Big Eddy and John Day stations (Dolan et al 1972) where ferroresonance was sustained by the energised parallel line. The motivation for the choice of this system is the occurrence of third harmonic steady state solution when the switching sequence was repeated during field test. The author is of the opinion that the third harmonic solution could be an isolated one. For the first system, investigations carried out to assess the effect of core loss nonlinearity on isolated subharmonic solutions are described. For the second system the sensitivity of isolated subharmonics with respect to length of the de-energised line is analysed. The analysis of fundamental ferroresonance and the sensitivity of the system with respect to length of the de-energised line have already been reported in Saravanaselvan et al (2005).

The state space equations that describe the dynamics of the ferroresonant circuits are derived using topological approach. Extensive

simulations have been carried out to analyse the range and stability of isolated subharmonic solutions. Analysis reveals the occurrence of supercritical and subcritical pitchfork bifurcations in the continuum of odd subharmonic solutions. The initial subharmonic steady states are obtained from temporal bifurcation diagrams. The local parameterisation based continuation algorithm is used to trace the entire subharmonic solution paths. Hybrid bifurcation diagrams are used to unearth the solutions hidden in subharmonic flip segments.

6.2 SYSTEMS DESCRIPTIONS AND COMPONENT MODELLING

The first system under investigation involves the 1100 kV transmission system of BPA. Ferroresonance occurred in this system during normal switching operation as reported in Dommel et al (1983). The three phase diagram of the system is shown in Fig.6.1a. The relevant data is given in Appendix 2. The shunt branch of the transformer equivalent circuit is represented by a nonlinear inductance (accounts for saturation) in parallel with a voltage controlled resistance (accounts for core loss). The core loss non linearity is modelled as per the method described in Neves and Dommel (1993). The third order polynomial (Equation 6.1) is used to describe the voltage controlled resistor. The coefficients of the polynomial are obtained using least square curve-fitting approach.

$$i_{Rm} = h_0 + h_1 v_{Lm} + h_2 v_{Lm}^2 + h_3 v_{Lm}^3 \qquad (6.1)$$

where,

v_{Lm} is the voltage across the transformer.

h_0, h_1, h_2, h_3 are the coefficients for core loss nonlinear function.

The saturation characteristic is represented by a two-term polynomial:

$$i_{Lm} = a\ \phi_{Lm} + b\ \phi_{Lm}^{q} \qquad (6.2)$$

where,

q is the degree of transformer saturation characteristic = 7,11.

a, b are the coefficients of nonlinear function which represent magnetisation characteristic.

ϕ_{Lm} is the transformer flux linkage.

The Thévenin equivalent circuit of the system is shown in Fig.6.1b. In this figure the voltage source E_{Th} and source impedance Z_{Th} constitute the Thévenin equivalent of the dashed portion of the system shown in Fig.6.1a. The topological approach is used to obtain the non redundant set of state variables that describe the circuit, Fig.6.1b.

The state variables chosen using topological approach are

$$x_1 = v_{C,}\ x_2 = i_t \text{ and } x_3 = \phi_{Lm}$$

where,

v_C is the voltage across the equivalent capacitor.

i_t is the transformer no-load current.

ϕ_{Lm} is the transformer flux linkage.

For the case of constant core loss resistance the dynamics of this circuit can be described by the following system of nonlinear differential equations:

$$\boldsymbol{p}x_1 = x_2/C_{Th} \qquad (6.3a)$$

$$\boldsymbol{p}x_2 = \{-x_1 - (R_2 + R_m)\ x_2 + a\ R_m\ x_3 + b\ R_m\ x_3^{q} + e_{Th}\}/L_2 \qquad (6.3b)$$

$$\boldsymbol{p}x_3 = R_m\ x_2 - a\ R_m\ x_3 - b\ R_m\ x_3^{q} = v_{Lm} \qquad (6.3c)$$

where,

$e_{Th} = E_{Th} \sin(\omega t)$.

For the case of nonlinear core loss resistance (voltage controlled resistance), the dynamics of this circuit can be described by the following system of nonlinear algebraic-differential equations:

$$i_{Rm} = f(v_{Lm}) = i_t - i_{Lm} = x_2 - a\, x_3 + b\, x_3^{q} \tag{6.4a}$$

$$\boldsymbol{p} x_1 = x_2 / C_{Th} \tag{6.4b}$$

$$\boldsymbol{p} x_2 = \{ - x_1 - v_{Lm} - R_2\, x_2 + e_{Th} \} / L_2 \tag{6.4c}$$

$$\boldsymbol{p} x_3 = v_{Lm} \tag{6.4d}$$

The second system under investigation involves a 525 kV transmission system of BPA between Big Eddy and John Day stations. The occurrence of ferroresonance in this system is reported in Dolan et al (1972). A brief description of the switching sequence that triggered ferroresonance is repeated here for convenience.

A three phase 1000 MVA 525/241.5 kV Y-connected bank of auto transformers, located at the Big Eddy Substation of Bonneville Power Administration (BPA) near The Dalles, Oregon, is connected on the 525 kV side through a disconnecting switch to 30.5 km of line and a circuit breaker is located at John Day Substation. A local circuit breaker is provided on the 230 kV bus at Big Eddy. Parallel and on the same right-of-way is the 525 kV John Day-Oregon City line. Over this length neither of the lines is transposed and C phase of the John Day-Big Eddy line is adjacent to A phase of the John Day-Oregon City line as shown in Fig.6.2a. When the Big Eddy line was cleared for line maintenance, immediately before the line was de-energized, the transformer load had been 170 MW and 140 MVAR into the 230 kV bus. The 525 kV circuit breaker at John Day was opened first and then the 230 kV circuit breaker at Big Eddy. Nine minutes later the gas accumulation alarm relay operated on C phase transformer.

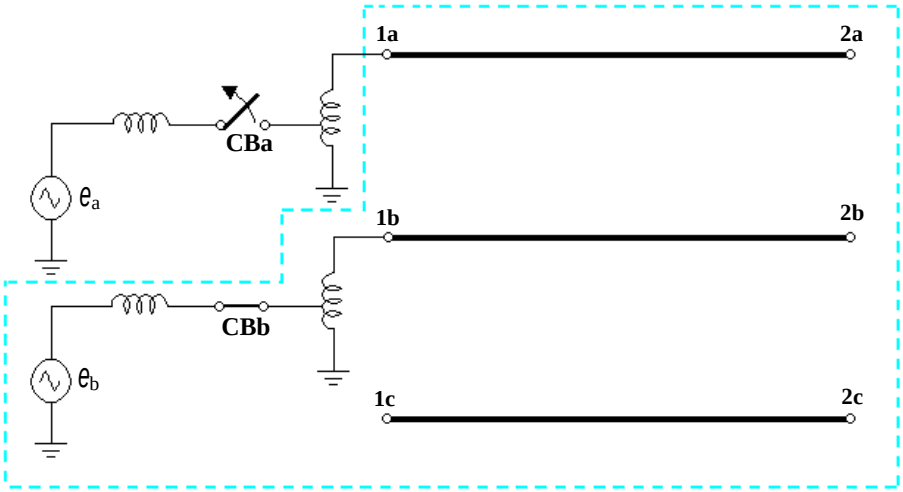

Fig.6.1a Three phase diagram for the 1100 kV system under study.

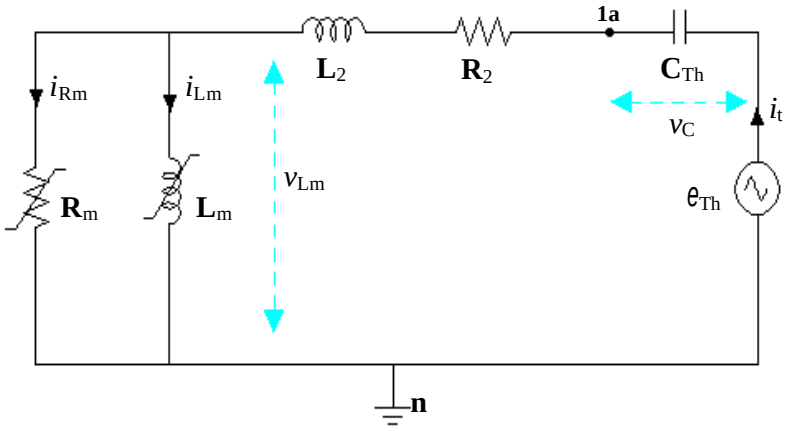

Fig.6.1b The circuit for ferroresonance investigations.

It took 7 to 13 minutes to disconnect the transformer from the line. So the transformer remained in ferroresonance between 16 to 22 min. The arching of C phase was much more severe than the other two phases.

Each phase of the unloaded autotransformer, Fig.6.2a, is represented by two parallel shunt branches. The first branch is modelled by a two-term polynomial of flux linkage, which accounts for saturation. The second branch is modelled by a linear resistance, which accounts for the core loss. The linear part of the system enclosed by the dashed lines in Fig.6.2a is reduced into a three phase Norton equivalent source and a capacitance matrix. The equivalent circuit of the system is shown in Fig.6.2b.

The topological approach is used to obtain the non-redundant set of state variables. The relevant proper tree is shown in Fig.6.3.
The chosen state variables are:

$x_1 = v_{CA}$; $x_2 = v_{CB}$; $x_3 = v_{CC}$;

$x_4 = \phi_{LmA}$; $x_5 = \phi_{LmB}$; $x_6 = \phi_{LmC.}$

The corresponding state equations are:

$$\begin{aligned} \boldsymbol{p}x_1 = {} & k_{11}x_1 + k_{12}x_2 + k_{13}x_3 + k_{14}\,a\,x_4 + k_{14}\,b\,x_4^{q} + k_{15}\,a\,x_5 + k_{15}\,b\,x_5^{q} \\ & + k_{16}\,a\,x_6 + k_{16}\,b\,x_6^{q} + k_{17}\,I_{NAp}\sin(\omega t+\theta_A) + k_{18}\,I_{NBp}\sin(\omega t+\theta_B) \\ & + k_{19}\,I_{NCp}\sin(\omega t+\theta_C) \end{aligned} \tag{6.5a}$$

$$\begin{aligned} \boldsymbol{p}x_2 = {} & k_{21}x_1 + k_{22}x_2 + k_{23}x_3 + k_{24}\,a\,x_4 + k_{24}\,b\,x_4^{q} + k_{25}\,a\,x_5 + k_{25}\,b\,x_5^{q} \\ & + k_{26}\,a\,x_6 + k_{26}\,b\,x_6^{q} + k_{27}\,I_{NAp}\sin(\omega t+\theta_A) + k_{28}\,I_{NBp}\sin(\omega t+\theta_B) \\ & + k_{29}\,I_{NCp}\sin(\omega t+\theta_C) \end{aligned} \tag{6.5b}$$

$$\begin{aligned} \boldsymbol{p}x_3 = {} & k_{31}x_1 + k_{32}x_2 + k_{33}x_3 + k_{34}\,a\,x_4 + k_{34}\,b\,x_4^{q} + k_{35}\,a\,x_5 + k_{35}\,b\,x_5^{q} \\ & + k_{36}\,a\,x_6 + k_{36}\,b\,x_6^{q} + k_{37}\,I_{NAp}\sin(\omega t+\theta_A) + k_{38}\,I_{NBp}\sin(\omega t+\theta_B) \\ & + k_{39}\,I_{NCp}\sin(\omega t+\theta_C) \end{aligned} \tag{6.5c}$$

$$\boldsymbol{p}x_4 = k_{41}\, x_1 + k_{42}\, a\, x_4 + k_{43}\, b\, x_4^{q} = v_{LmA} \quad (6.5d)$$

$$\boldsymbol{p}x_5 = k_{51}\, x_2 + k_{52}\, a\, x_5 + k_{53}\, b\, x_5^{q} = v_{LmB} \quad (6.5e)$$

$$\boldsymbol{p}x_6 = k_{61}\, x_3 + k_{62}\, a\, x_6 + k_{63}\, b\, x_6^{q} = v_{LmC} \quad (6.5f)$$

where,

v_{CA}, v_{CB} and v_{CC} are the voltages across the capacitors C_{gA}, C_{gB} and C_{gC}.

ϕ_{LmA}, ϕ_{LmB} and ϕ_{LmC} are the flux linkages of the transformers.

v_{LmA}, v_{LmB} and v_{LmC} are the voltages across the transformers.

q is the degree of transformer saturation characteristic = 7,11.

a, b are the coefficients of nonlinear function which represent magnetisation characteristic.

I_{NAp}, I_{NBp} and I_{NCp} are the peak values of the Norton sources.

$\boldsymbol{p}$ is the time derivative operator.

The value of circuit parameters considered for investigation and the coefficients k are given in Appendix 3.

6.3 TIME DOMAIN SIMULATION AND VALIDATION

Equations (6.5a) to (6.5f) are integrated using fourth order Runge-Kutta method (RK4). Figures 6.4a and 6.4b show the steady state time domain responses obtained from MicroTran and fourth order Runge-Kutta method respectively. As can be seen, the results match perfectly.

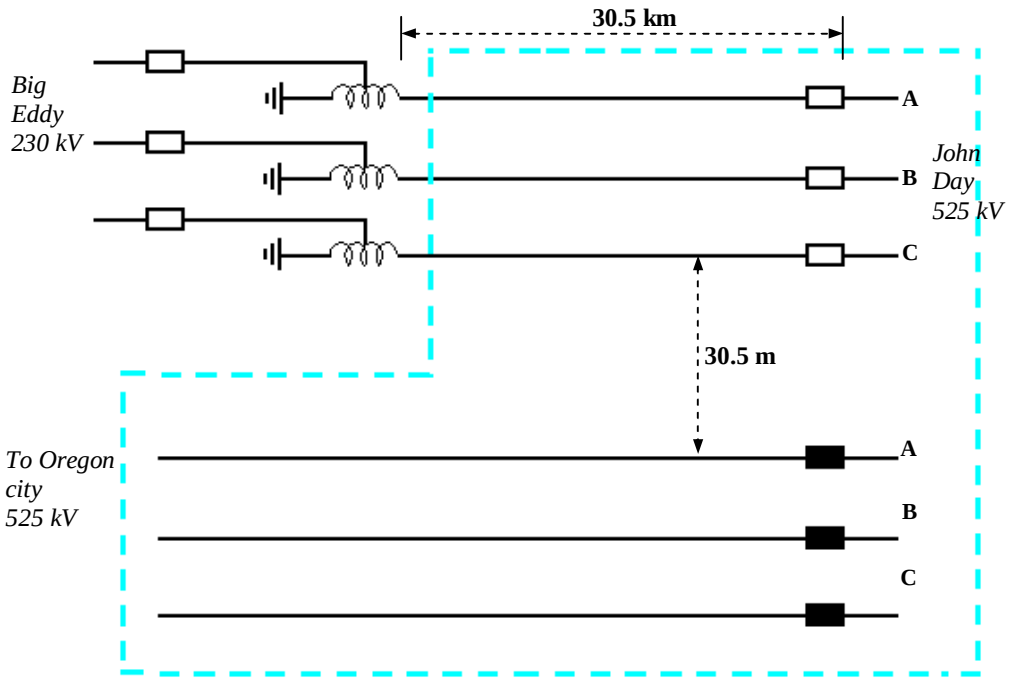

Fig.6.2a Three phase diagram of 525 kV transmission system between Big Eddy and John Day stations (Dolan et al 1972).

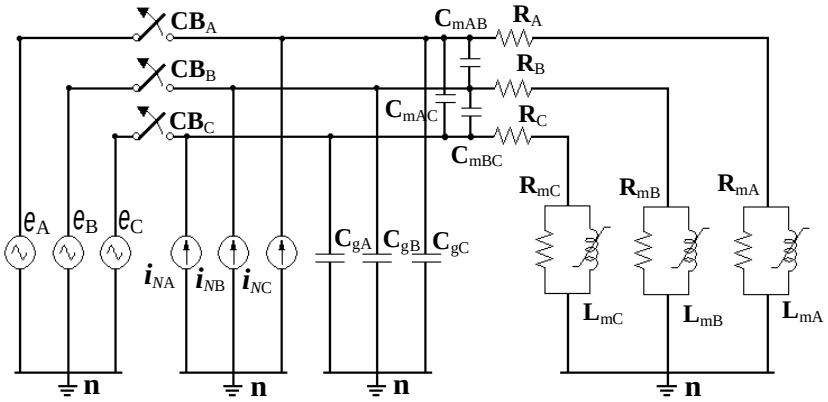

Fig.6.2b Equivalent circuit for ferroresonance investigations.

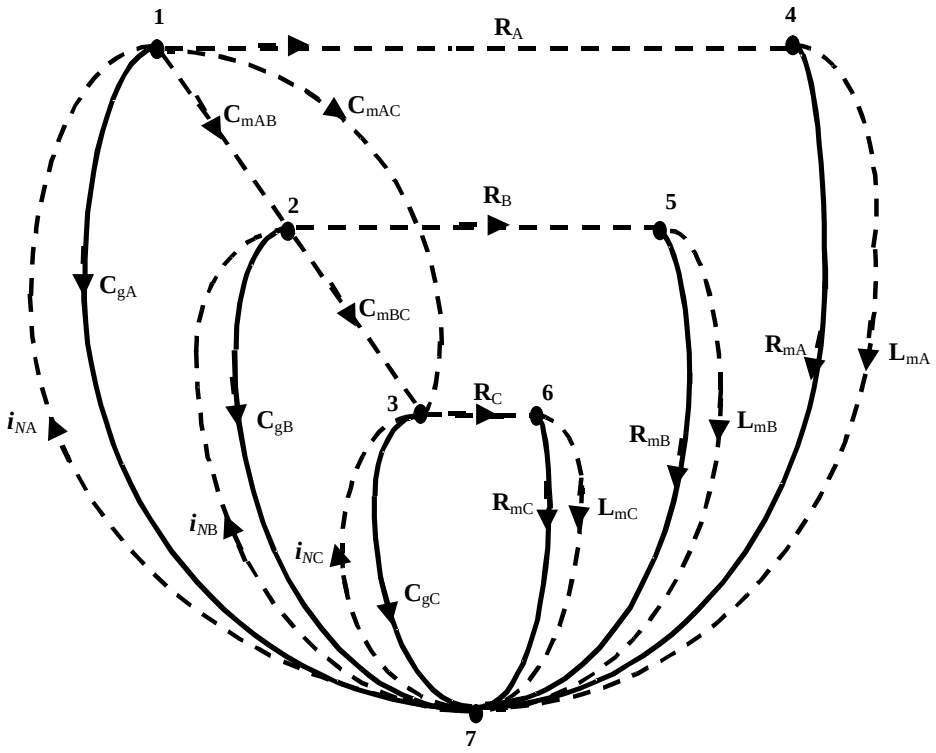

Fig.6.3 A proper tree for the circuit of Fig.6.2b.

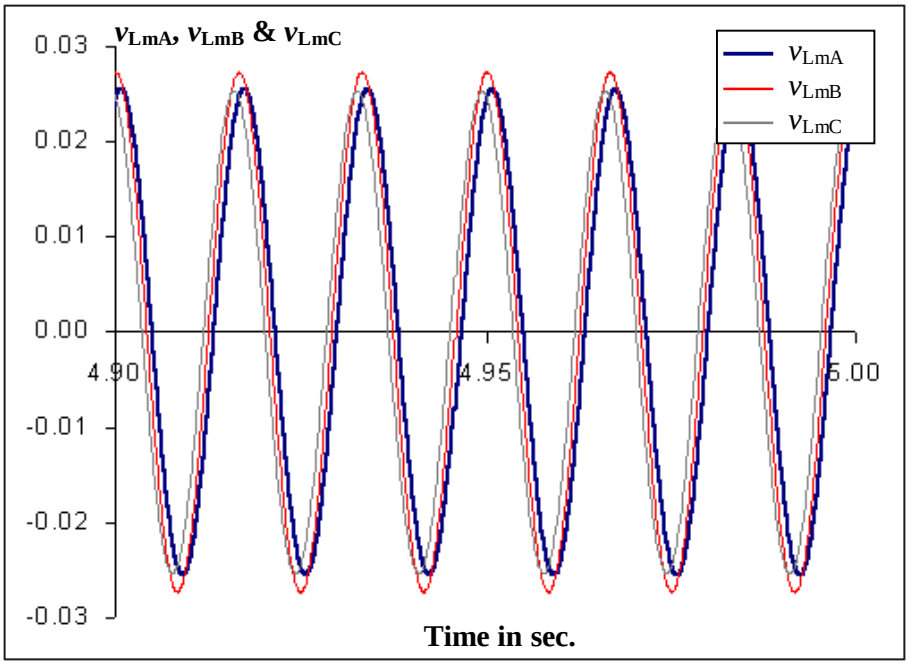

Fig.6.4a Time plot of the voltage across the transformers (v_{LmA}, v_{LmB} and v_{LmC}) from RK4: linear core loss model, I_{Np} = 1.0 A, q = 7.
Initial condition: $x_1(0)$ = 0 V, $x_2(0)$ = 0 V, $x_3(0)$ = 0 V, $x_4(0)$ = 0 Vsec, $x_5(0)$ = 0 Vsec, $x_6(0)$ = 0 Vsec.

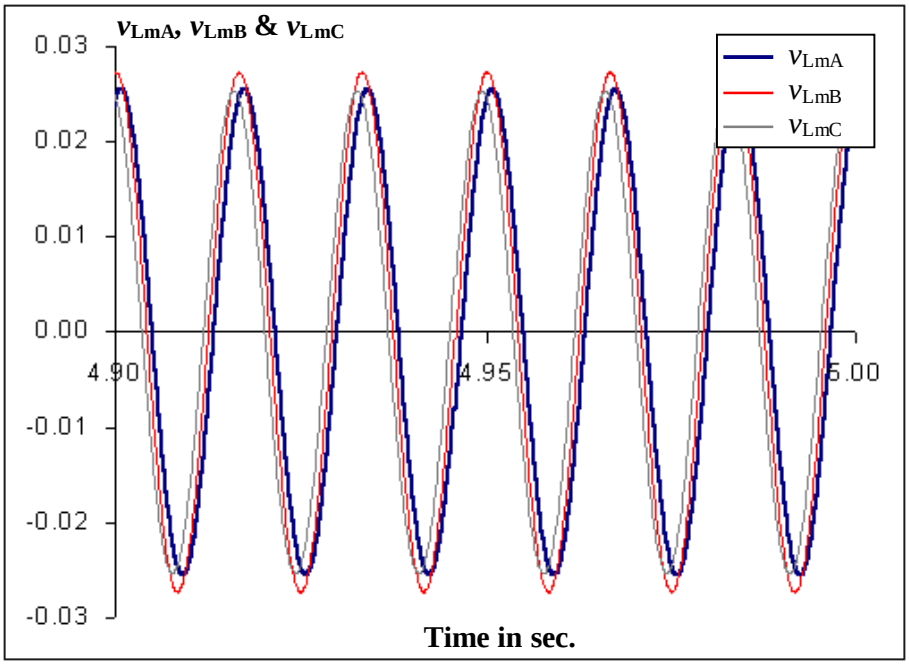

Fig.6.4b Time plot of the voltage across the transformers (v_{LmA}, v_{LmB} and v_{LmC}) from MicroTran: linear core loss model, I_{Np} = 1.0 A, q = 7.
Initial condition: $v_{CA}(0)$ = 0 V, $v_{CB}(0)$ = 0 V, $v_{CC}(0)$ = 0 V, $\phi_A(0)$ = 0 Vsec, $\phi_B(0)$ = 0 Vsec, $\phi_C(0)$ = 0 Vsec.

6.4 EFFECT OF CORE LOSS NONLINEARITY – 1100 kV SYSTEM OF BPA

This section describes investigations carried out to assess the isolated subharmonic behaviour of the circuit shown in Fig.6.1b for both linear and nonlinear core loss model. Also, the sensitivity of the state variable with respect to the saturation level of the core is presented. Temporal bifurcation diagrams and bifurcation diagrams of the steady state solutions are used for the analysis of isolated subharmonic solutions.

6.4.1 Temporal bifurcation diagram

The cases considered for investigations are summarised in Case matrix A.1, Table 6.1. Temporal bifurcation diagrams are generated for the cases given in Case matrix A.1. The periodicity of solutions obtained from temporal bifurcation diagrams for different cases are given in Table 6.2. The results entered in this table are to be associated with the case numbers in the corresponding positions in Table 6.1.

Table 6.1 Case matrix A.1: Cases considered for analysis.

q / Core loss	Linear	Nonlinear
7	A.1.1	A.1.2
11	A.1.3	A.1.4

Table 6.2 Result matrix B.1: Periodicity of solutions obtained.

q / Core loss	Linear	Nonlinear
7	P_2, P_3, P_5, P_7, P_9 and P_{21} Fig.6.5	P_2 Fig.6.6
11	P_2, P_3, P_5, P_7 and P_9 Fig.6.7	P_2 Fig.6.8

Figures 6.5 to 6.8 show the temporal bifurcation diagrams for the cases in Case matrix A.1. It can be observed from figures that the nonlinearity in core loss significantly damps the subharmonic oscillations. Time domain plots of typical fundamental and subharmonic solutions are presented in Figures 6.9 to 6.13.

Table 6.3 shows the peak values of source and transformer voltages for different fundamental and subharmonic solutions. The ratios between peaks of source and transformer voltages are also given in the table. It is to be noted that the peak of period 5 response is almost 400% of the peak of source.

Table 6.3 Ratios between peaks of source and transformer voltages.

Periodicity of solution (Figure No.)	Peak value of the source voltage in p.u.	Peak value of voltage across the transformer in p.u.	Ratio between peaks
Period 1 (Fig.6.9a)	1.2	1.664562	1.387135
Period 2 (Fig.6.9c)	0.79	2.157799	2.731391
Period 3 (Fig.6.10a)	1.16	2.486507	2.143540
Period 5 (Fig.6.10c)	0.68	2.708934	3.983726
Period 7 (Fig.6.11a)	1.2	3.199039	2.665865
Period 9 (Fig.6.11b)	1.24	2.952092	2.380719
Period 21 (Fig.6.13)	1.27	3.149009	2.479534

The continuum of each subharmonic solution is obtained using the local parameterisation based continuation technique.

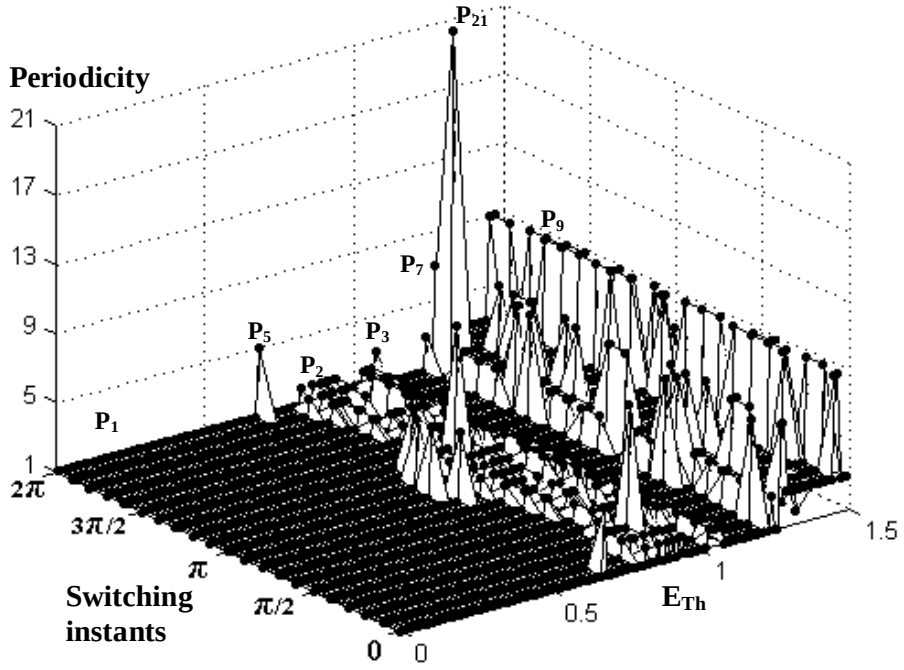

Fig.6.5 Temporal bifurcation diagram for Case A.1.1. (q = 7, linear core loss model).

P_1 – fundamental solution, P_2, P_3, P_5, P_7, P_9 and P_{21} – isolated subharmonic solutions.

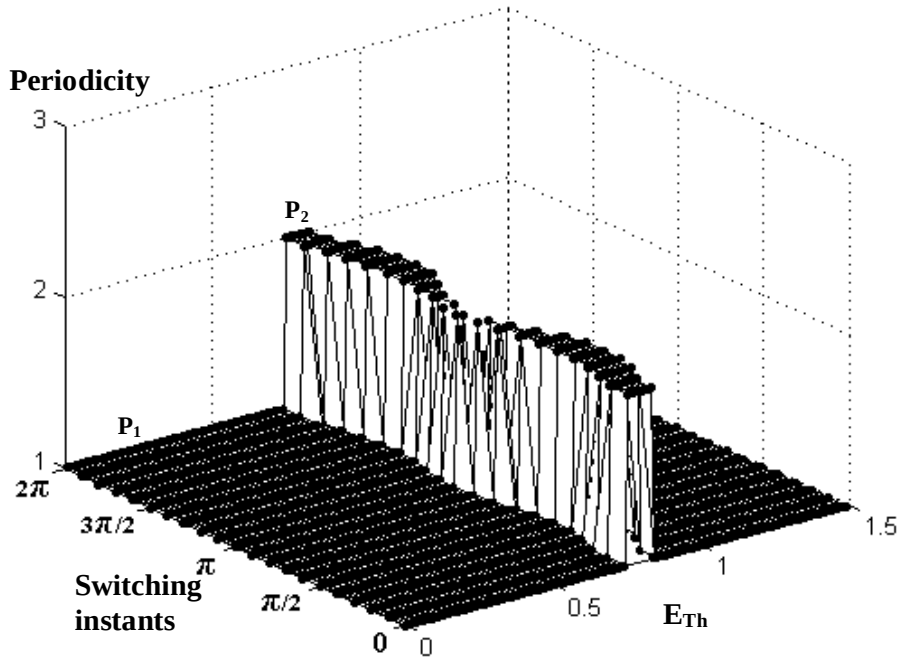

Fig.6.6 Temporal bifurcation diagram for Case A.1.2 (q = 7, nonlinear core loss model).

P_1 – fundamental solution and P_2 – isolated subharmonic solution.

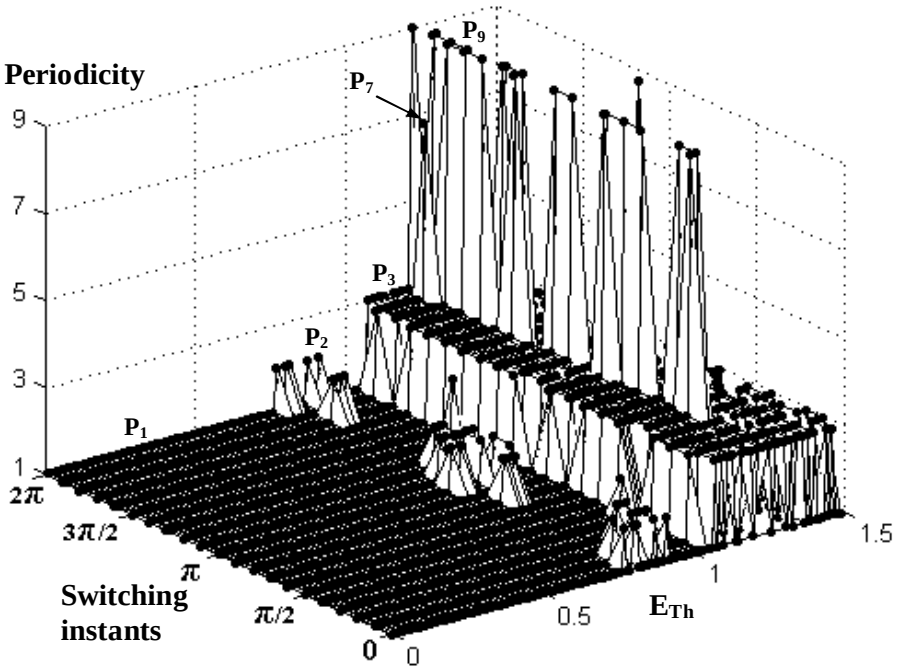

Fig.6.7 Temporal bifurcation diagram for Case A.1.3 (q = 11, linear core loss model).

P_1 – fundamental solution, P_2, P_3, P_7 and P_9 – isolated subharmonic solutions.

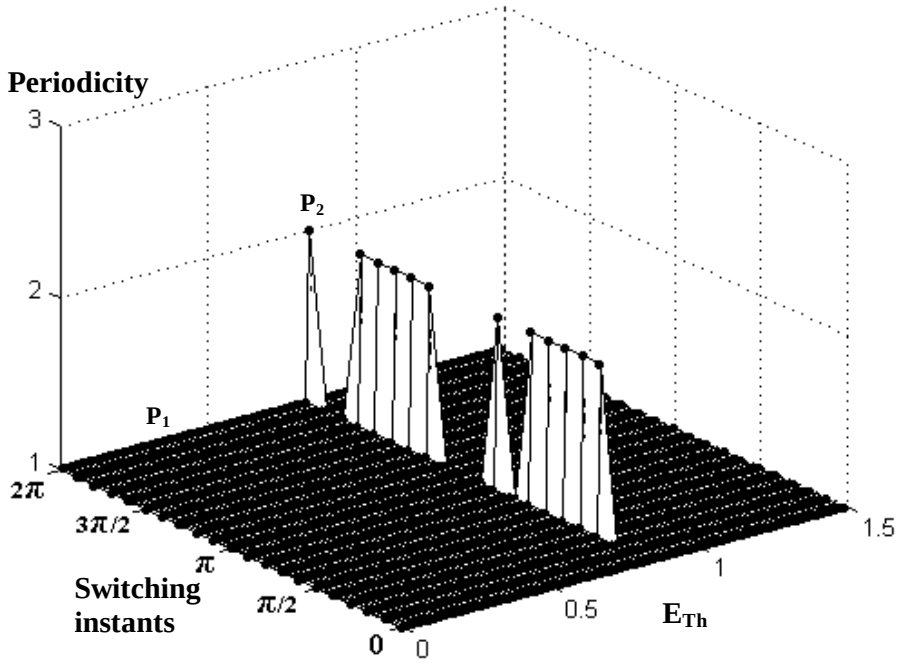

Fig.6.8 Temporal bifurcation diagram for Case A.1.4 (q = 11, nonlinear core loss model).

P_1 – fundamental solution and P_2 – isolated subharmonic solution.

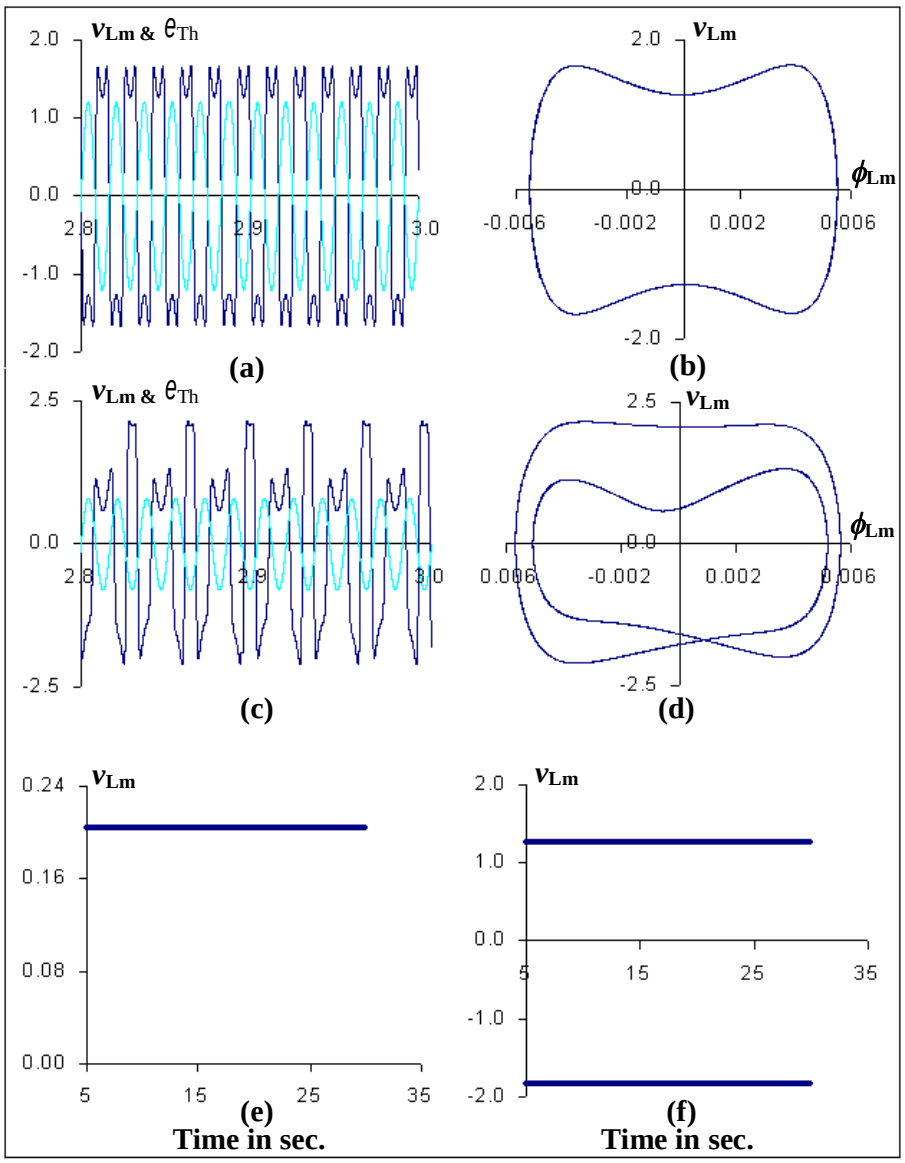

Fig.6.9 Time plots, phase plots and evolving Poincaré maps. Initial conditions are obtained from temporal bifurcation diagram, Fig.6.5.

(a) Time domain plot of P_1 oscillation at E_{Th} = 1.20 p.u., Case A.1.1.
(b) Phase plot of P_1 oscillation, Fig.6.9a.
(c) Time domain plot of P_2 oscillation at E_{Th} = 0.79 p.u., Case A.1.1.
(d) Phase plot of P_2 oscillation, Fig.6.9c.
(e) Evolving Poincaré map of P_1 oscillation, Fig.6.9a.
(f) Evolving Poincaré map of P_2 oscillation, Fig.6.9c.

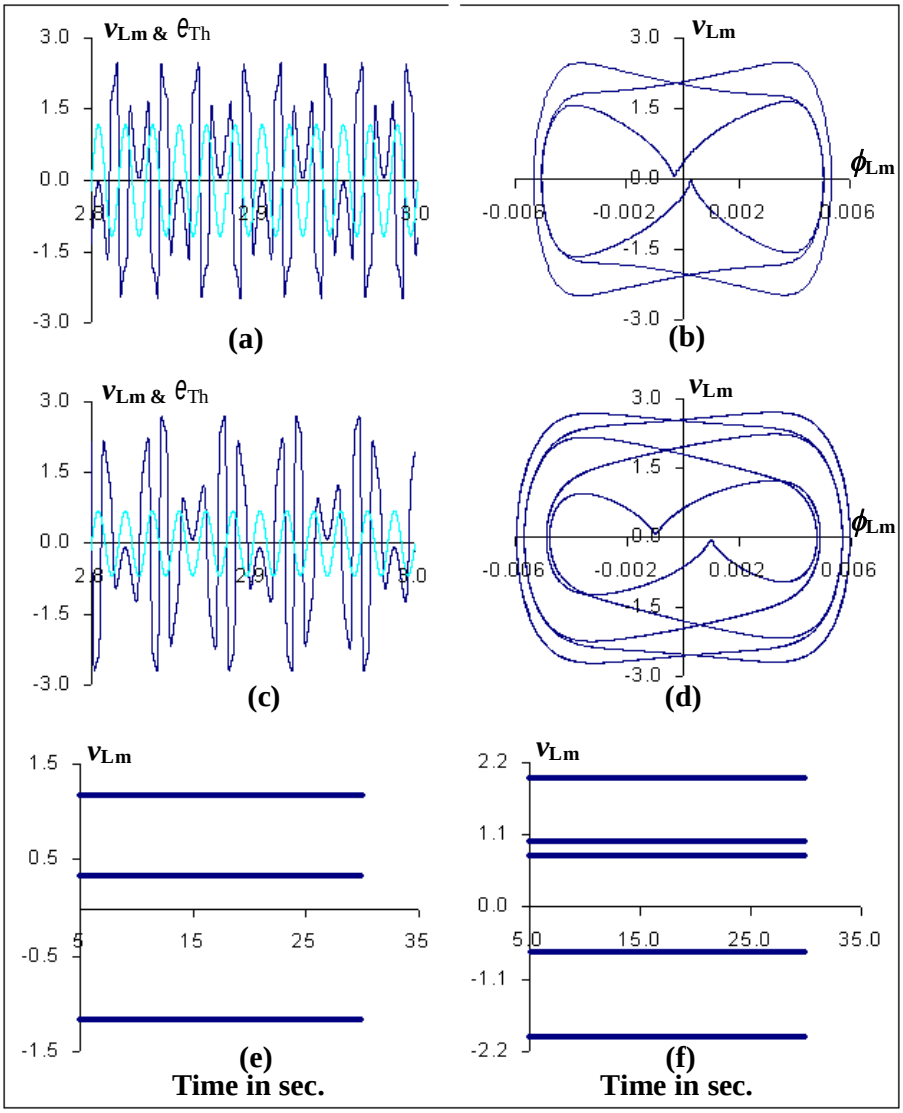

Fig.6.10 Time plots, phase plots and evolving Poincaré maps. Initial conditions are obtained from temporal bifurcation diagram, Fig.6.7.

(a) Time domain plot of P_3 oscillation at E_{Th} = 1.16 p.u., Case A.1.3.
(b) Phase plot of P_3 oscillation, Fig.6.10a.
(c) Time domain plot of P_5 oscillation at E_{Th} = 0.68 p.u., Case A.1.3.
(d) Phase plot of P_5 oscillation, Fig.6.10c.
(e) Evolving Poincaré map of P_3 oscillation, Fig.6.10a.
(f) Evolving Poincaré map of P_5 oscillation, Fig.6.10c.

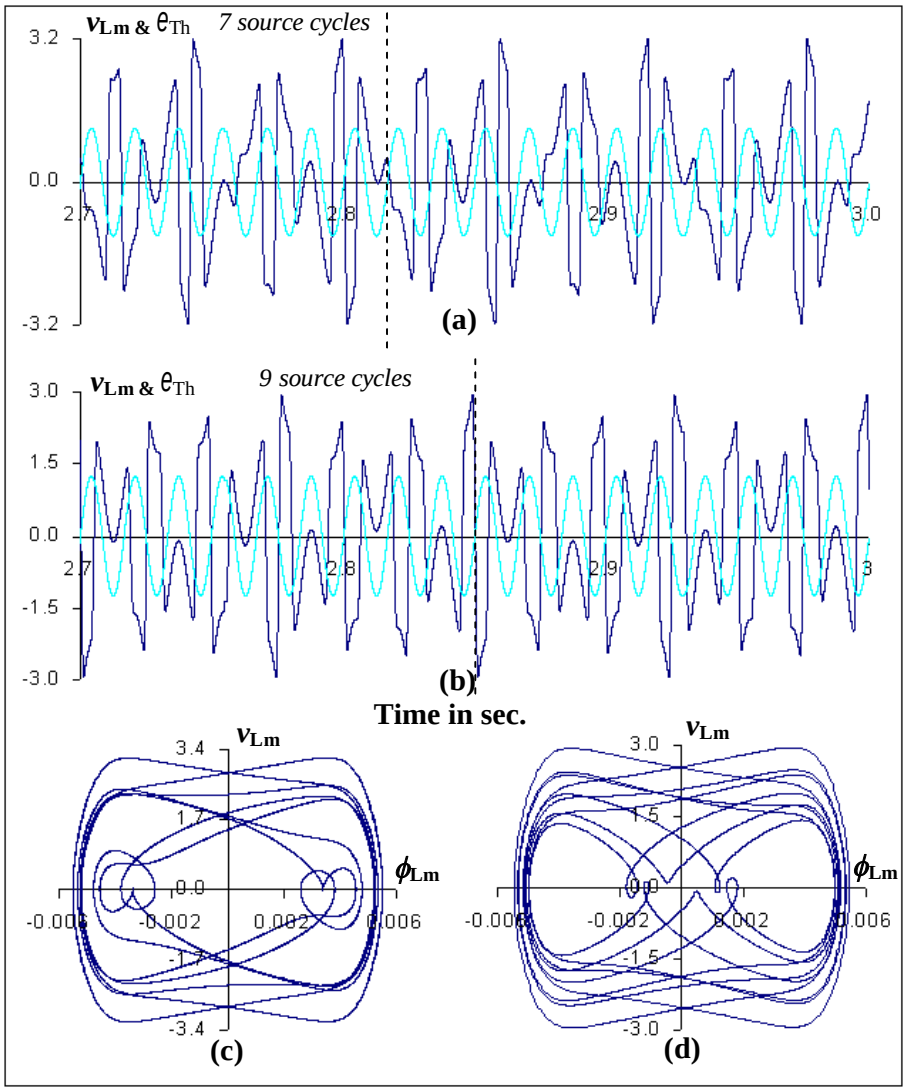

Fig.6.11 Time domain and phase plots of P_7 and P_9 oscillations. Initial conditions are obtained from temporal bifurcation diagram, Fig.6.7.

(a) Time plot of P_7 oscillation at E_{Th} = 1.20 p.u., Case A.1.3.
(b) Time plot of P_9 oscillation at E_{Th} = 1.24 p.u., Case A.1.3.
(c) Phase plot of P_7 oscillation, Fig.6.11a.
(d) Phase plot of P_9 oscillation, Fig.6.11b.

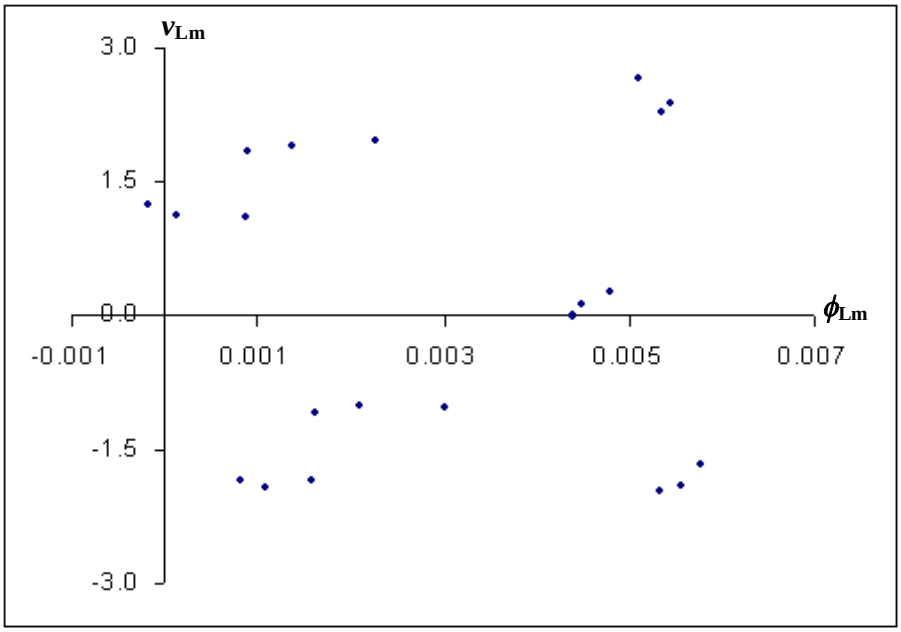

Fig.6.12 Conventional Poincaré map of P_{21} oscillation at E_{Th} = 1.27 p.u. of Fig.6.5.

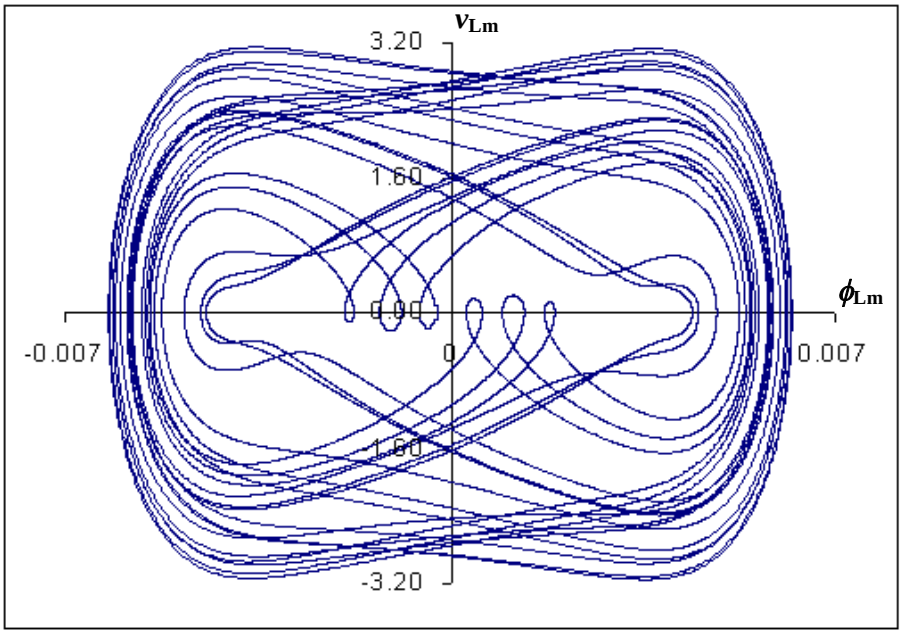

Fig.6.13 Phase plot corresponding to Fig.6.12.

6.4.2 Bifurcation diagram of steady state isolated subharmonic solutions

Figures 6.14 and 6.15 show the bifurcation diagram of period 2 solutions for different transformer core saturation indices. The bifurcation diagrams of period 3 solutions for different core saturation indices are given in Fig.6.16 and Fig.6.17. It can be observed that subharmonic solutions occur at a lower value of bifurcation parameter for higher transformer saturation index. Higher core saturation index also increases the number of bifurcations. Supercritical pitchfork bifurcations are identified in the continuum of period 3 solution (**PF_1, PF_2, PF_3** and **PF_4** in Figures 6.16 and 6.17). Table 6.4 shows the peak values of Thévenin source voltage at which different bifurcations occur. It confirms the occurrence of bifurcations at lower parameter values for higher core saturation index.

Table 6.4 Peak values of Thévenin source voltage in p.u. at different bifurcation points in the continuum of period 3 solution, Case A.1.1 and Case A.1.3.

q / Bifurcation points	**PF_1**	**PF_2**	**PF_3**	**PF_4**
7	1.661762	1.978088	1.618828	2.017515
11	1.334225	2.006725	1.362531	1.888893

Figures 6.18a to 6.18f show the phase plots of different symmetric and non symmetric period 3 oscillations around bifurcation points PF_1, PF_3 and PF_4 of Fig.6.17.

The bifurcation diagram of steady state period 5 solution is shown in Fig.6.19. Supercritical pitchfork bifurcation is encountered in this case too. In figure, the symmetric P_5 solution loses its symmetry at two points (PF_1 and PF_2 in Fig.6.15). The symmetry breaking bifurcation point PF_1 is followed by two non symmetric P_5 solution branches PF_1 - a_1 and PF_1 - b_1. The point PF_2 is followed by two non symmetric P_5 solution branches PF_2 - a_2 and PF_2 - b_2. The phase plots of symmetric and non symmetric solutions are shown in Fig.6.20. The Fourier spectrums of the same are shown in Figures 6.21 and 6.22. As expected, for the symmetric period 5 solution the Fourier spectrum contains spikes only at the odd multiples of base frequency (60 / 5 = 12 Hz), Fig.6.21. In case of the non symmetric period 5 solution, Fourier spectrum contains spikes at both odd and even multiples of base frequency, Fig.6.22.

The continua of period 7 solutions for different transformer core saturation indices are given in Figures 6.23 and 6.24. Figures confirm the existence of more bifurcations for higher core saturation index. Fig.6.25 depicts the magnified view of box A in Fig.6.23. Interestingly, the non symmetric branches of period 7 solution are not followed by flip segments. The stable symmetric solution loses its symmetry at PF_1 and thereby two stable non symmetric branches appear. Further, these two branches meet at point PF_2 and the non symmetric solution gains its symmetry. Figure 6.26 shows the phase plots of symmetric and non symmetric period 7 solutions.

The bifurcation diagram of period 9 solutions is shown in Fig.6.27. The phase plots of symmetric and non symmetric P_9 solutions around supercritical pitchfork bifurcation point PF_1 are shown in Fig.6.28a and Fig.6.28b.

Figures 6.29 and 6.30 depict the bifurcation diagram of period 2 solutions obtained with nonlinearity in core loss. With nonlinearity in core loss included only period 2 subharmonic solutions exist, Figures 6.6 and 6.8. It can be observed from Figures 6.29 and 6.30 that higher core saturation index increases the range of period 2 solutions and reduces the existence of stable period 2 solutions. Figures 6.31a to 6.31d show the phase plots of different P_2, P_4 solutions in segments P_{2a}, P_{2c}, P_{2e} and F of Fig.6.29. Fig.6.32 depicts the time plot of P_4 solution, Fig.6.31d, superimposed on the source waveform. Figures 6.33a to 6.33d show the phase plots of different P_2, P_4 solutions in segments P_{2a}, P_{2b} , P_{2c} and F of Fig.6.30. Fig.6.34 depicts the time plot of P_2 solution, Fig.6.30a, superimposed on the source waveform.

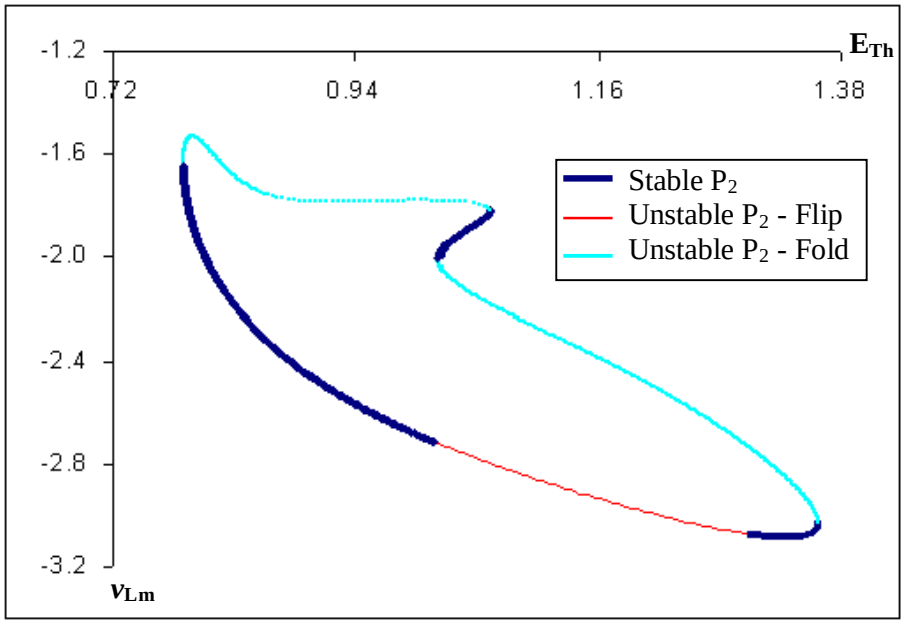

Fig.6.14 Bifurcation diagram of steady state period 2 solution, Case A.1.1 (q = 7, linear core loss model). Initial condition is obtained from temporal bifurcation diagram, Fig.6.5.

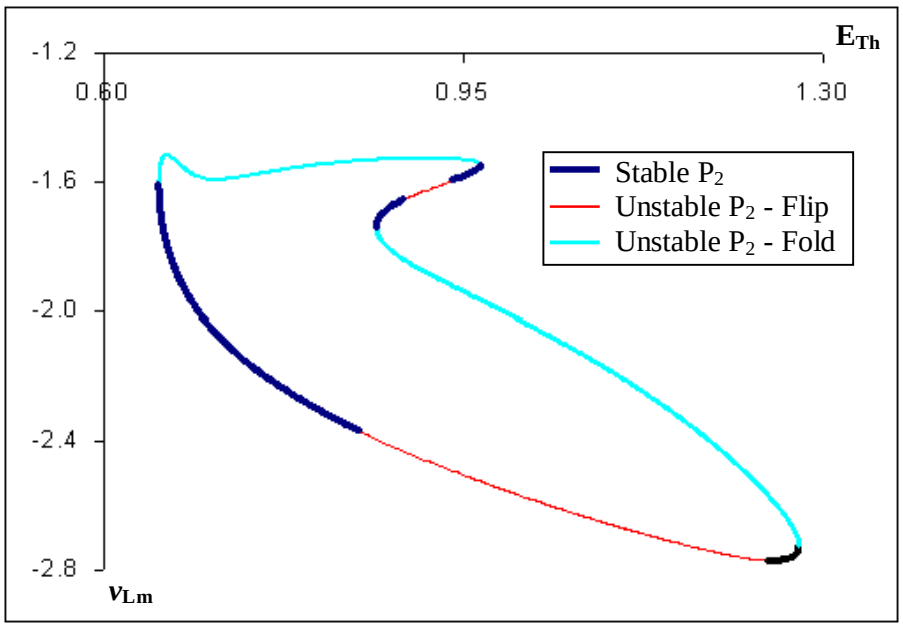

Fig.6.15 Bifurcation diagram of steady state period 2 solution, Case A.1.3 (q = 11, linear core loss model). Initial condition is obtained from temporal bifurcation diagram, Fig.6.7.

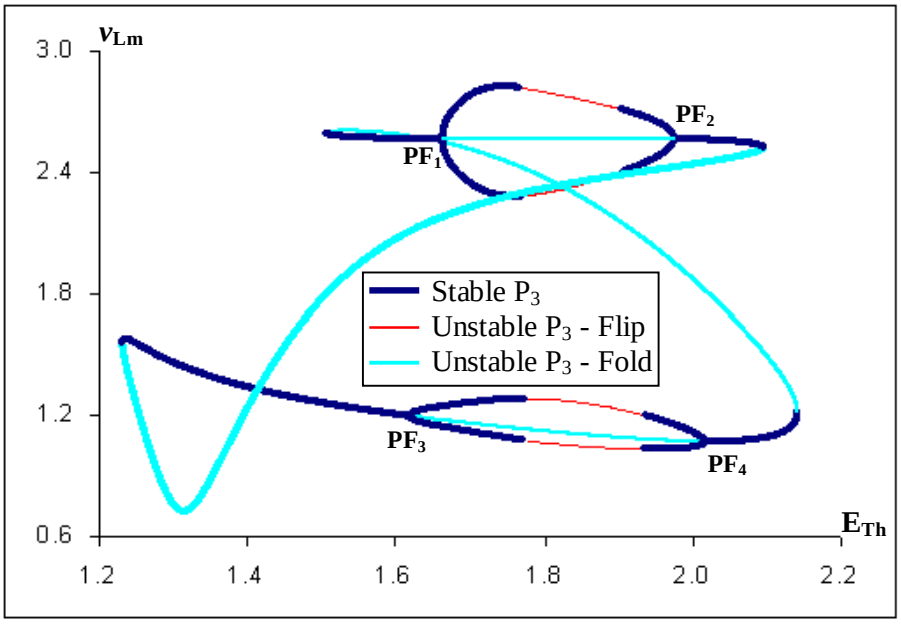

Fig.6.16 Bifurcation diagram of steady state period 3 solution, Case A.1.1 (q = 7, linear core loss model). PF – supercritical pitchfork bifurcation point. Initial condition is obtained from temporal bifurcation diagram, Fig.6.5.

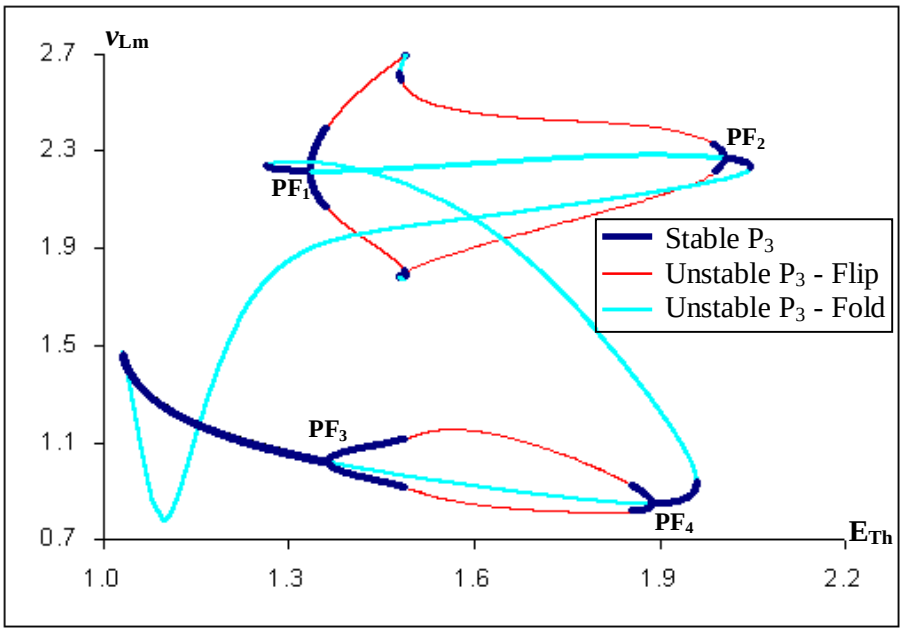

Fig.6.17 Bifurcation diagram of steady state period 3 solution, Case A.1.3 (q = 11, linear core loss model). PF – supercritical pitchfork bifurcation point. Initial condition is obtained from temporal bifurcation diagram, Fig.6.7.

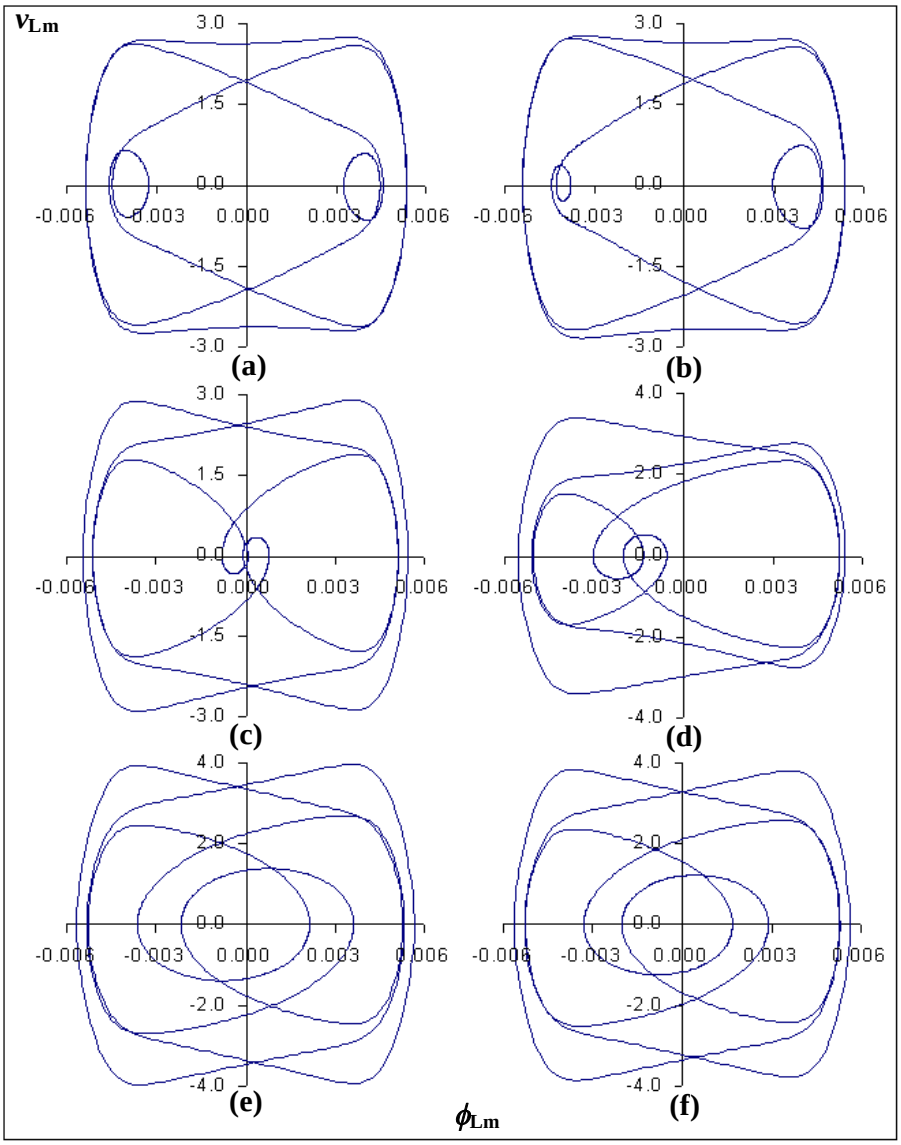

Fig.6.18 Phase plots of symmetric and non symmetric period 3 solutions.

(a) Symmetric P_3 solution at E_{Th} = 1.30672 p.u. around PF_1 of Fig.6.17.
(b) Non symmetric P_3 solution at E_{Th} = 1.35815 p.u. around PF_1 of Fig.6.17.
(c) Symmetric P_3 solution at E_{Th} = 1.34003 p.u. around PF_3 of Fig.6.17.
(d) Non symmetric P_3 solution at E_{Th} = 1.47400 p.u. around PF_3 of Fig.6.17.
(e) Symmetric P_3 solution at E_{Th} = 1.95693 p.u. around PF_4 of Fig.6.17.
(f) Non symmetric P_3 solution at E_{Th} = 1.88191 p.u. around PF_4 of Fig.6.17.

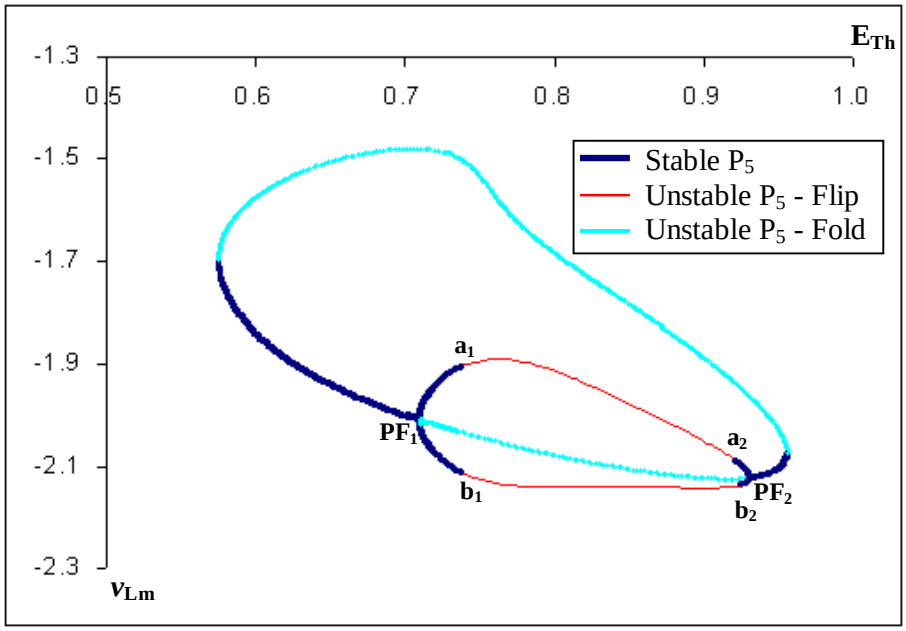

Fig.6.19 Bifurcation diagram of steady state period 5 solution, Case A.1.1 (q = 7, linear core loss model). PF – supercritical pitchfork bifurcation point. Initial condition is obtained from temporal bifurcation diagram, Fig.6.5.

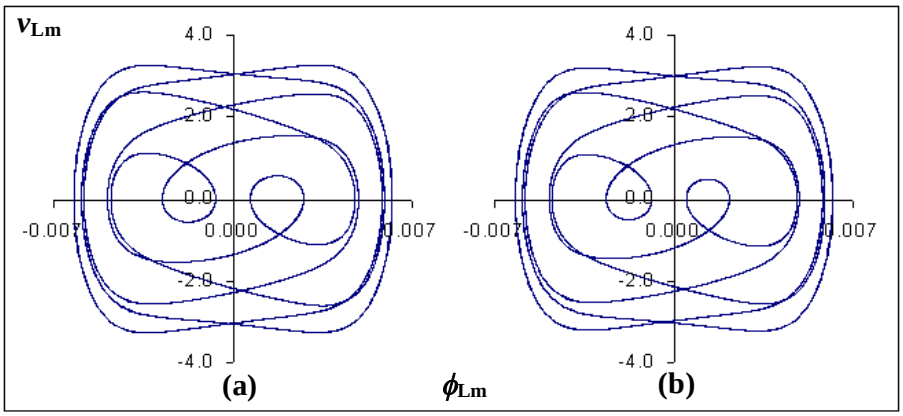

Fig.6.20 Phase plots of symmetric and non symmetric P_5 oscillations.

(a) Symmetric P_5 solution at E_{Th} = 0.95302 p.u. around PF_2 of Fig.6.19.

(b) Non symmetric P_5 solution at E_{Th} = 0.92415 p.u. around PF_2 of Fig.6.19.

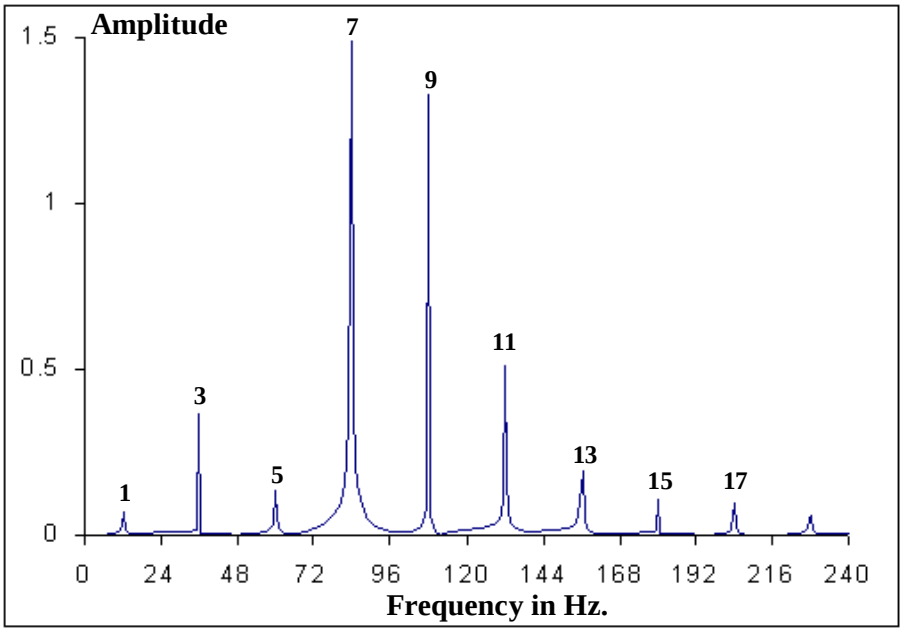

Fig.6.21 Fourier spectrum of symmetric period 5 oscillation, Fig.6.20a. The numbers above peaks denote the multiples of base frequency = 60/5 = 12 Hz.

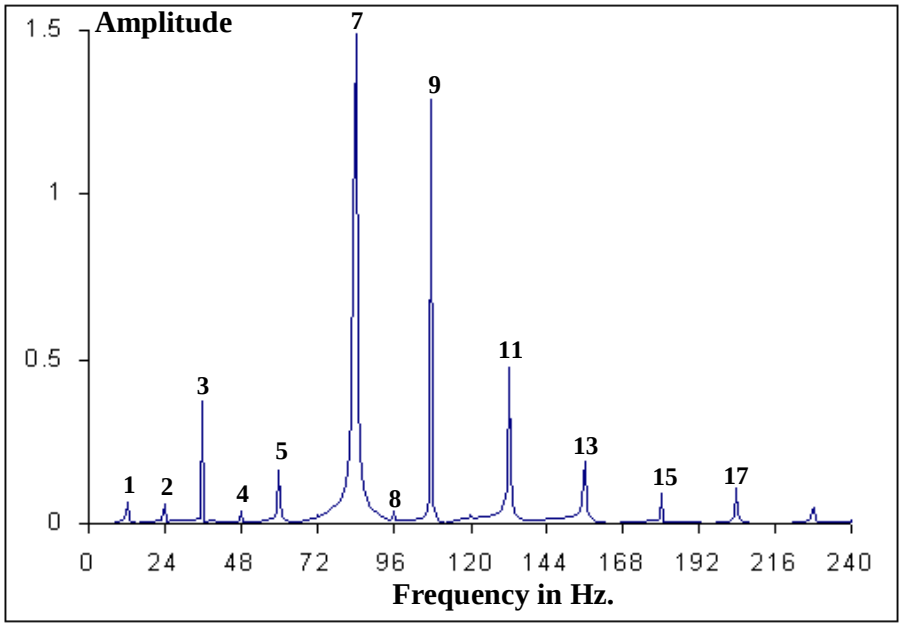

Fig.6.22 Fourier spectrum of non symmetric period 5 oscillation, Fig.6.21b. The numbers above peaks denote the multiples of base frequency = 60/5 = 12 Hz.

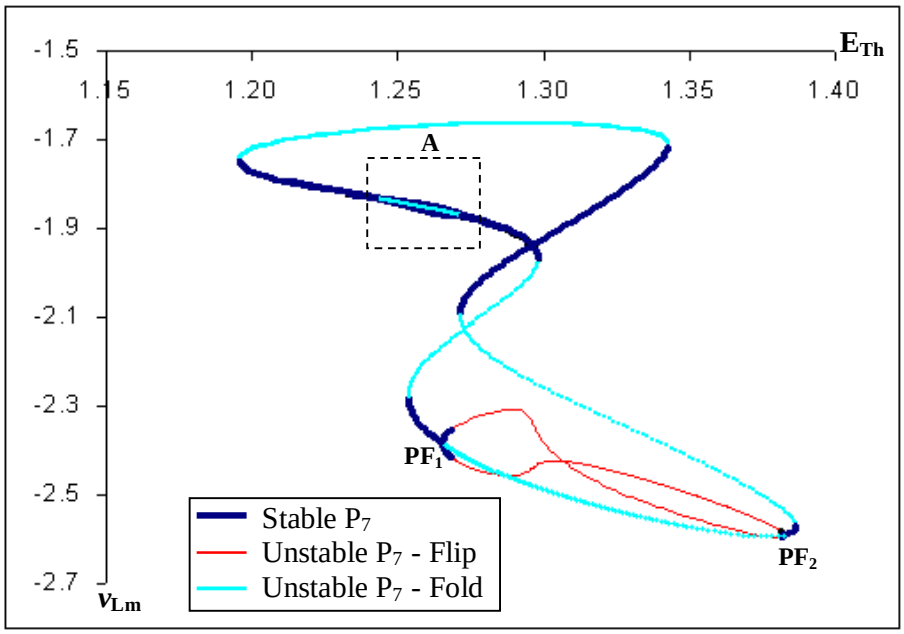

Fig.6.23 Bifurcation diagram of steady state period 7 solution, Case A.1.1 (q = 7, linear core loss model). PF – supercritical pitchfork bifurcation point. Initial condition is obtained from temporal bifurcation diagram, Fig.6.5.

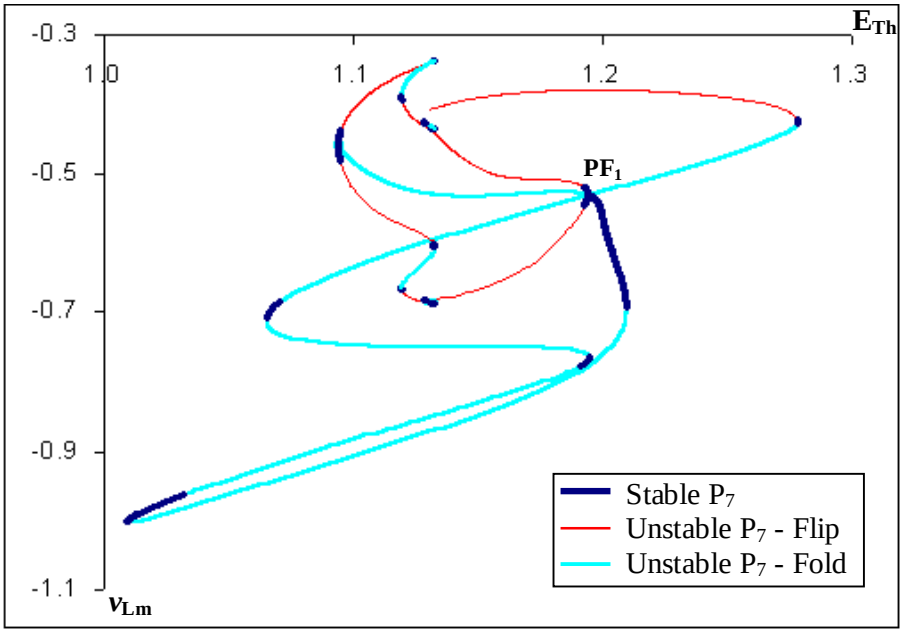

Fig.6.24 Bifurcation diagram of steady state period 7 solution, Case A.1.3 (q = 11, linear core loss model). PF – supercritical pitchfork bifurcation point. Initial condition is obtained from temporal bifurcation diagram, Fig.6.7.

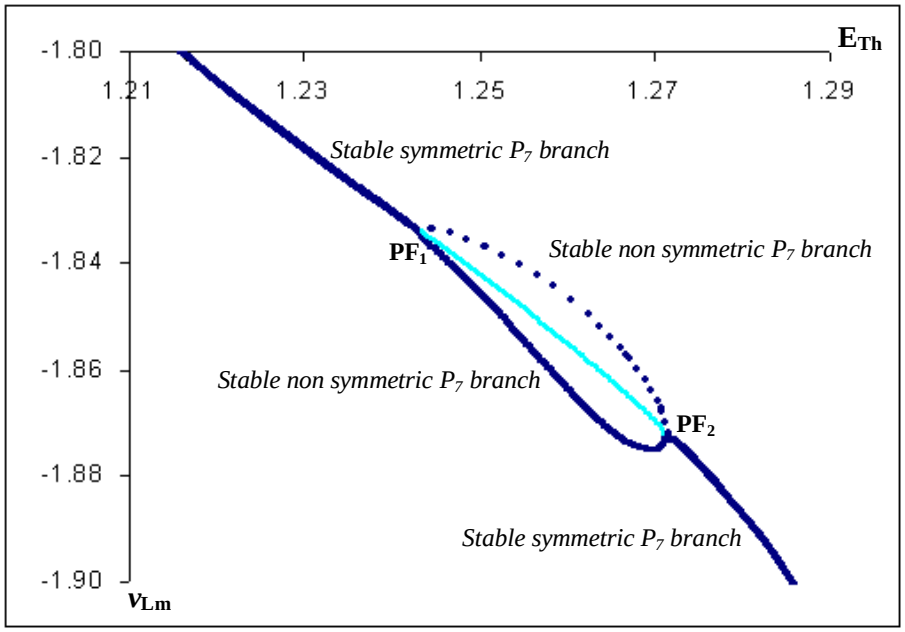

Fig.6.25 Magnification of region A of Fig.6.23. PF – supercritical pitchfork bifurcation point.

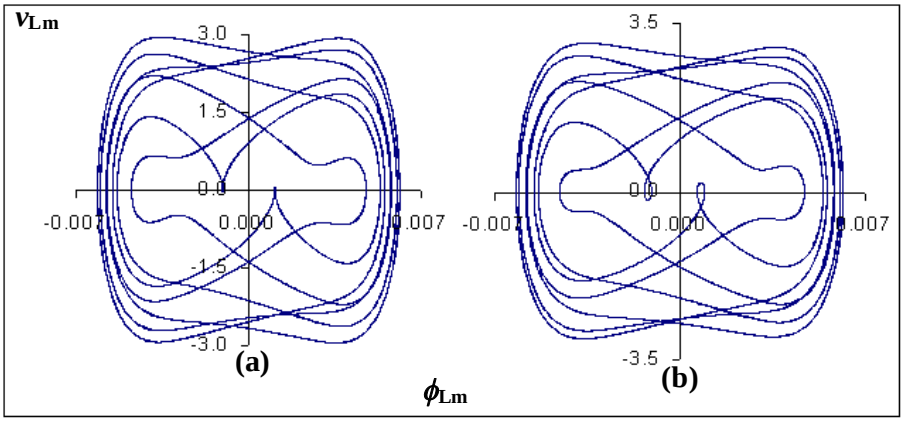

Fig.6.26 Phase plots of period 7 subharmonic oscillations.

(a) Symmetric P_7 solution at E_{Th} = 1.226365 p.u. around PF_1 of Fig.6.25.

(b) Non symmetric P_7 solution at E_{Th} = 1.265975 p.u. around PF_1 of Fig.6.25.

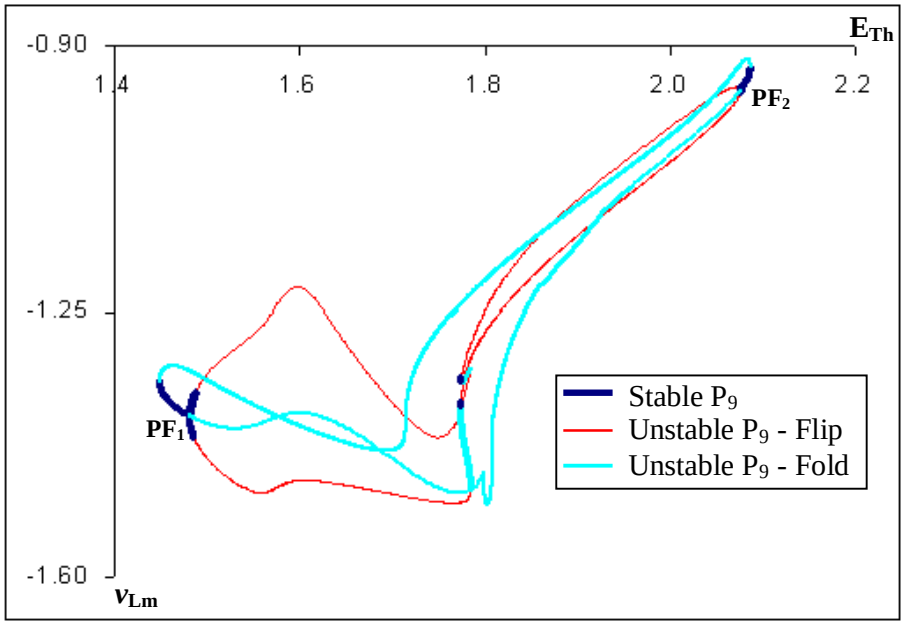

Fig.6.27 Bifurcation diagram of steady state period 9 solution, Case A.1.1 (q = 7, linear core loss model). PF – supercritical pitchfork bifurcation point. Initial condition is obtained from temporal bifurcation diagram, Fig.6.5.

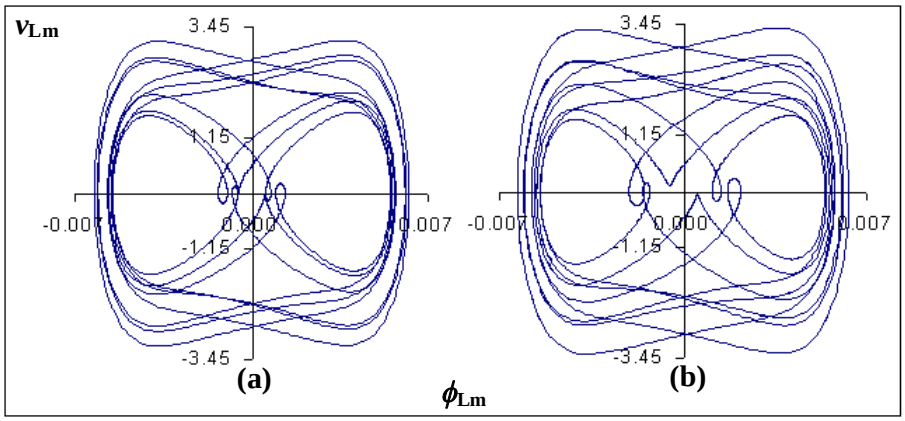

Fig.6.28 Phase plot of period 9 subharmonic oscillations.

(a) Symmetric P_9 solution at E_{Th} = 1.449964 p.u. around PF_1 of Fig.6.27.

(b) Non symmetric P_9 solution at E_{Th} = 1.483855 p.u. around PF_1 of Fig.6.27.

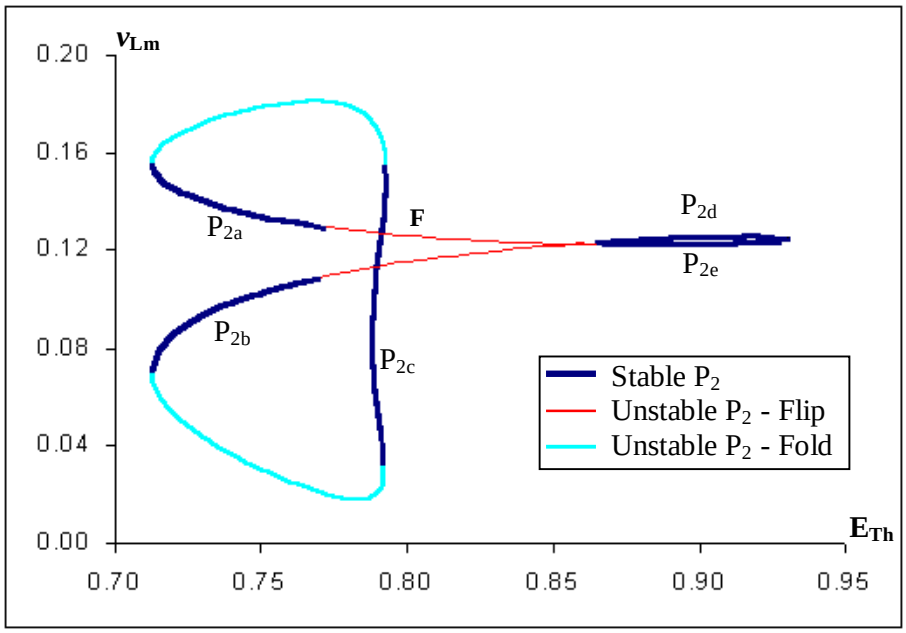

Fig.6.29 Bifurcation diagram of steady state period 2 solution, Case A.1.2 (q = 7, nonlinear core loss model). P_{2a} to P_{2e} - different stable period 2 solution segments.

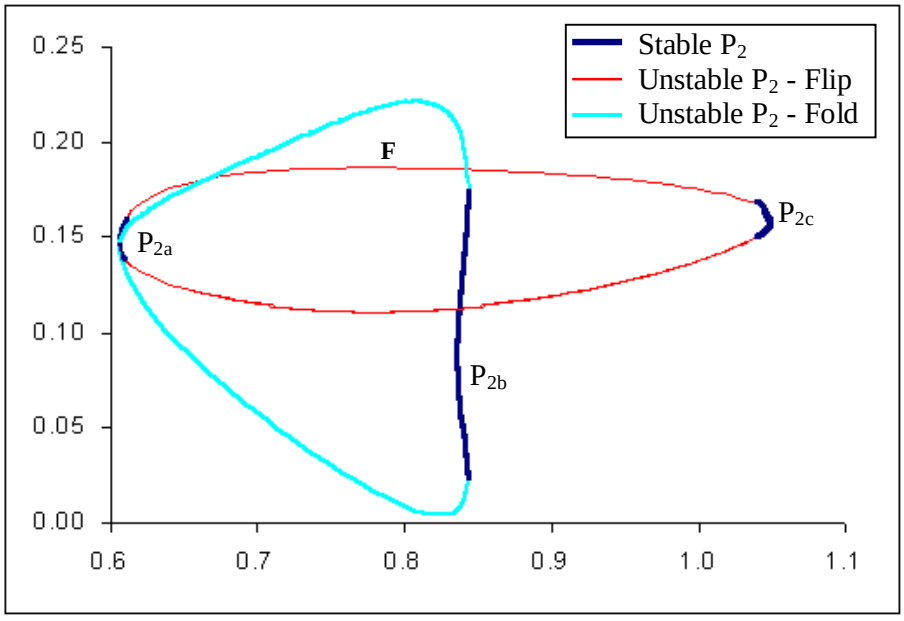

Fig.6.30 Bifurcation diagram of steady state period 2 solution, Case A.1.4 (q = 11, nonlinear core loss model). P_{2a} to P_{2c} - different stable period 2 solution segments.

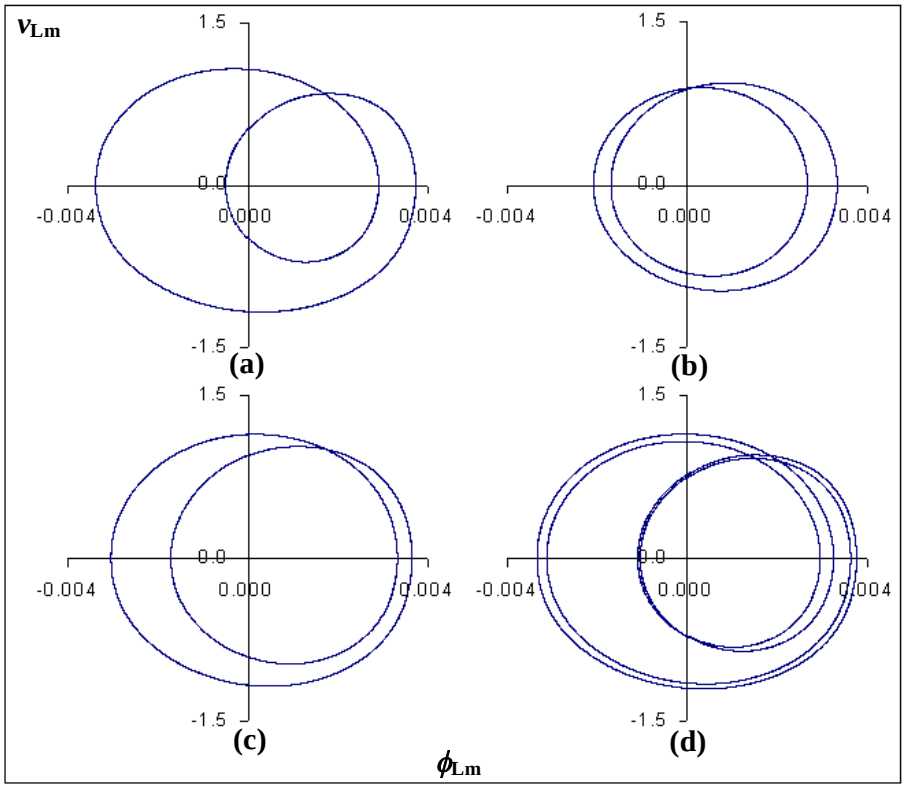

Fig.6.31 Phase plot of period 2 and period 4 oscillations.

(a) P_2 solution at E_{Th} = 0.762302 p.u. (in P_{2a} of Fig.6.29)
(b) P_2 solution at E_{Th} = 0.791158 p.u. (in P_{2c} of Fig.6.29)
(c) P_2 solution at E_{Th} = 0.892302 p.u. (in P_{2e} of Fig.6.29)
(d) P_4 solution at E_{Th} = 0.827302 p.u. (in F of Fig.6.29)

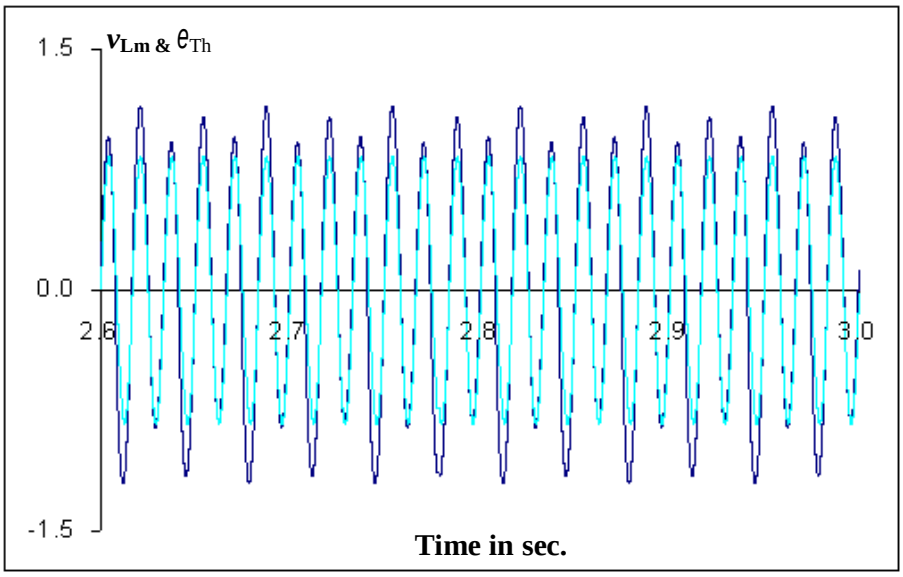

Fig.6.32 Time domain plot of period 4 oscillation, Fig.6.32d, superimposed on source waveform.

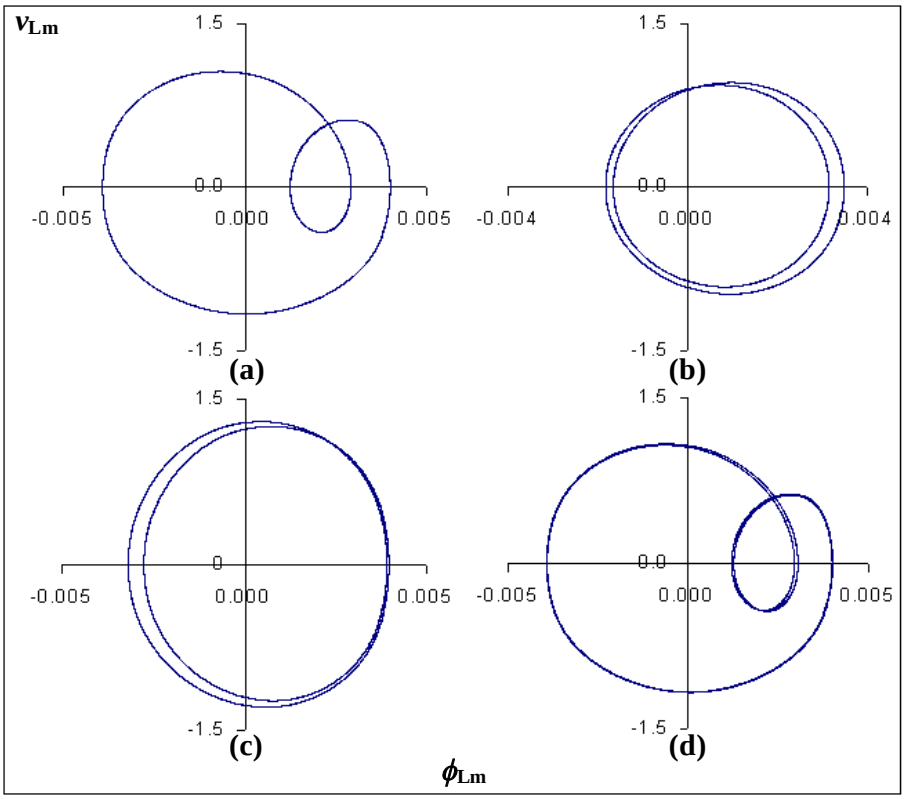

Fig.6.33 Phase plot of period 2 subharmonic oscillations.

(a) P_2 solution at E_{Th} = 0.60697 p.u. (in P_{2a} of Fig.6.30)
(b) P_2 solution at E_{Th} = 0.836094 p.u. (in P_{2b} of Fig.6.30)
(c) P_2 solution at E_{Th} = 1.044486 p.u. (in P_{2c} of Fig.6.30)
(d) P_4 solution at E_{Th} = 0.615526 p.u. (in F of Fig.6.30)

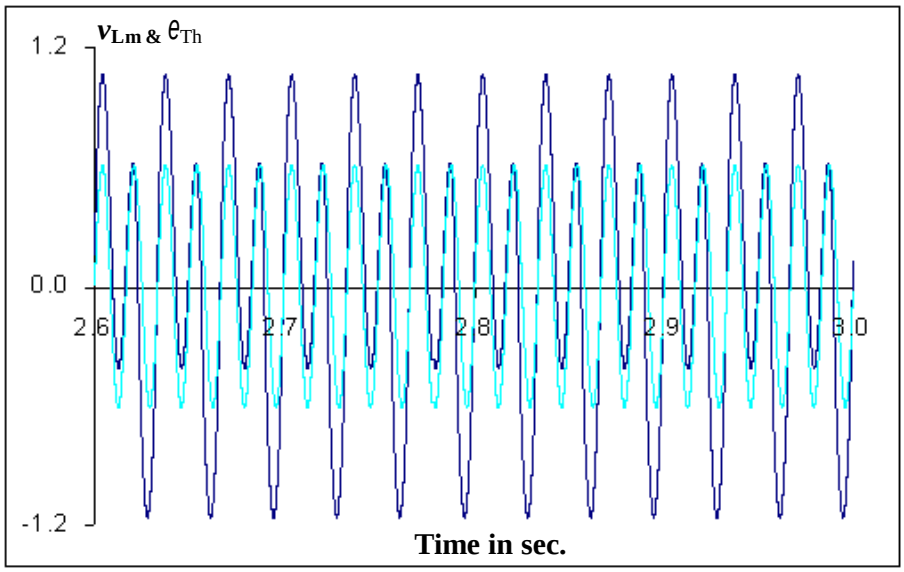

Fig.6.34 Time domain plot of period 2 oscillation, Fig.6.34a, superimposed on source waveform.

6.5 EFFECT OF LENGTH OF DE-ENERGISED LINE – 525 kV SYSTEM OF BPA

This section describes investigations carried out on isolated subharmonic solutions in a transformer-terminated line due to an energised parallel line in the same right-of-way. The equivalent circuit shown in Fig.6.2b is analysed to unravel isolated subharmonics and its sensitivity with respect to capacitance to ground of the de-energised line, transformer saturation and amplitude of Norton's current source. The capacitance to ground of the de-energized line is directly proportional to the line length. The sensitivity of the isolated subharmonics with respect to the length of the de-energized line is obtained by changing its capacitance to ground. Temporal bifurcation diagrams and bifurcation diagrams of the steady state solutions are used for the analysis of behaviour of isolated subharmonics.

6.5.1 Temporal bifurcation diagram

Temporal bifurcation diagrams have been generated for several cases with various combinations of circuit parameters. Only the representative cases are presented here. Figures 6.35a to 6.35d show the temporal bifurcation diagrams for different core saturations and capacitances to ground. It can be seen from the figures that only fundamental solutions exist for the range of I_{Np} considered for lower saturation index. Figures 6.35b and 6.35d correspond to higher saturation index, which bring out the isolated subharmonic solutions (P_2, P_3, P_5 and P_7). It is also to be noted from the figures that longer the de-energized line (more capacitance to ground) more is the tendency towards periodic behaviour. In other words, for longer de-energised lines the onset of chaos occurs at a higher value of bifurcation parameter (I_{Np}).

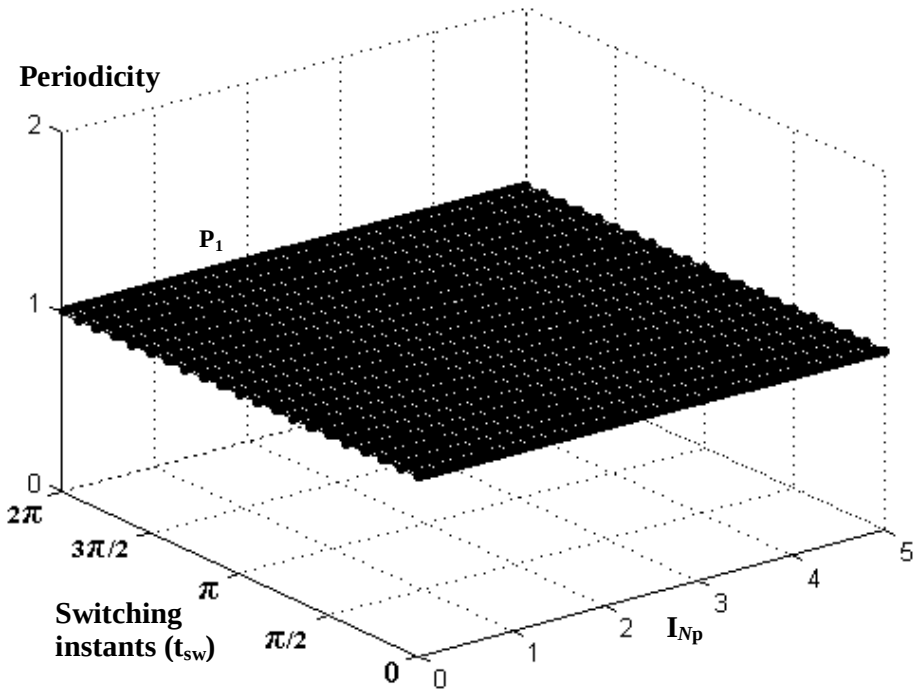

Fig.6.35a Temporal bifurcation diagram: q = 7, C_g = 100% of base case value, linear core loss model.
P_1 – fundamental solution.

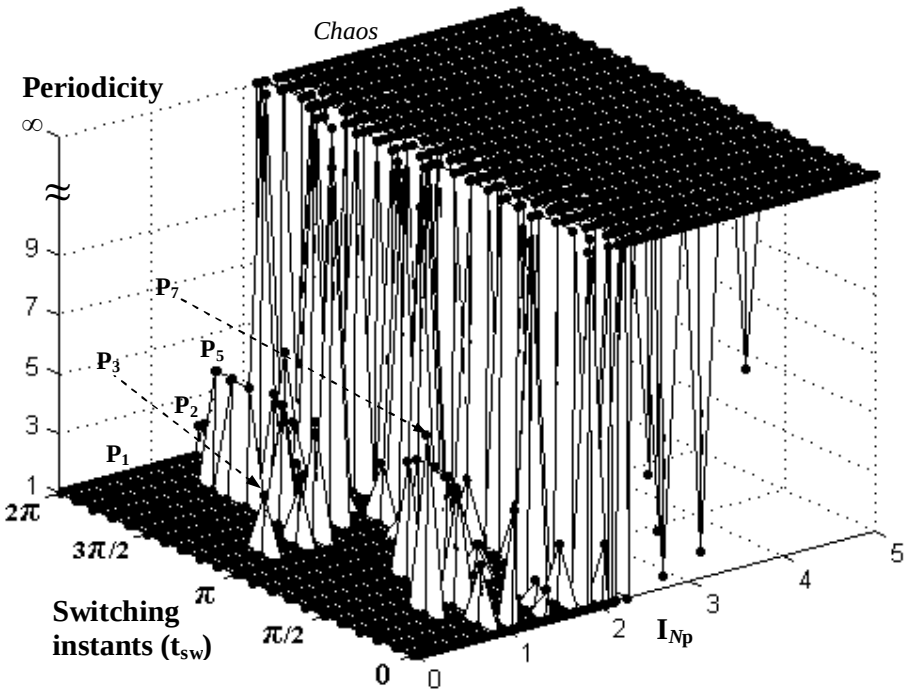

Fig.6.35b Temporal bifurcation diagram: q = 11, C_g = 100% of base case value, linear core loss model.
P_1 – fundamental solution, P_2, P_3, P_5 and P_7 – isolated subharmonic solutions.

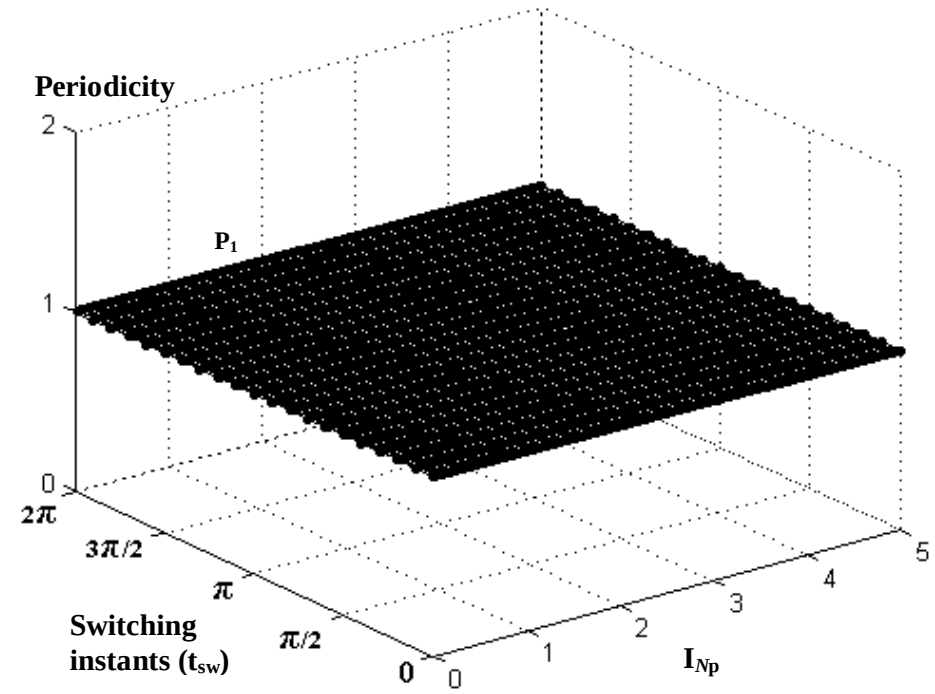

Fig.6.35c Temporal bifurcation diagram: q = 7, C_g = 200% of base case value, linear core loss model.
P_1 – fundamental solution.

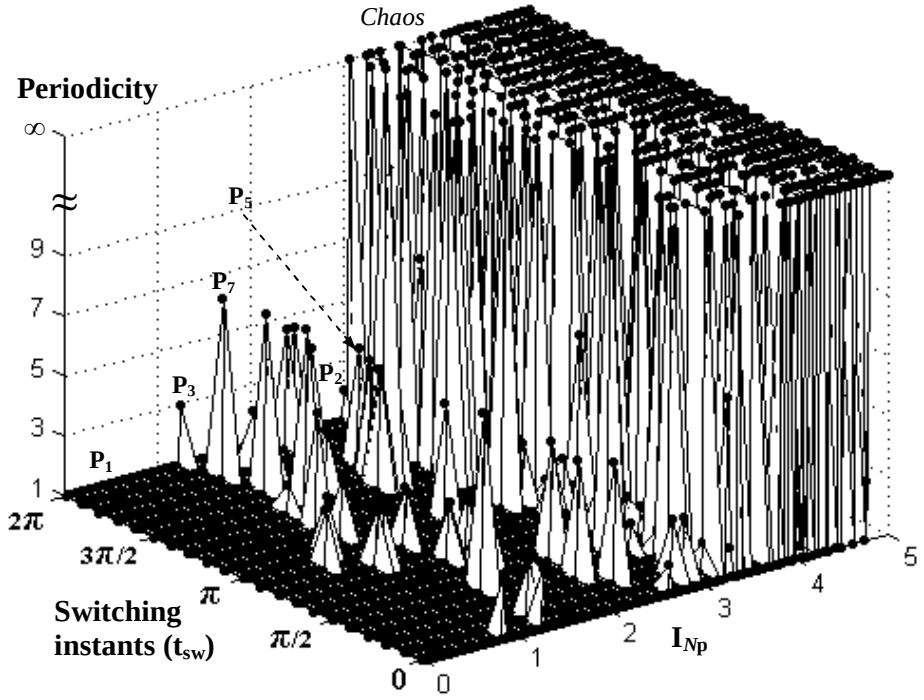

Fig.6.35d Temporal bifurcation diagram: q = 11, C_g = 200% of base case value, linear core loss model.
P_1 – fundamental solution, P_2, P_3, P_5 and P_7 – isolated subharmonic solutions.

Figures 6.36 to 6.38 show the time domain and phase plots of fundamental ferroresonant solutions. It is important to note that the field test reported in Dolan et al (1972) indicates that only phase C of the transformer experienced high-amplitude ferroresonant oscillations. However the time plots reveal that high-amplitude ferroresonant oscillations are not restricted to phase C, Figures 6.38a and 6.38b.

The time domain and phase plots of isolated subharmonic and chaotic solutions are shown in Figures 6.39 to 6.43. As can be seen, the period 5 and period 7 solutions posses symmetry, Fig.6.43b and Fig.6.43d. The continuum of each subharmonic solution is traced by the continuation procedure. The results obtained are presented in the next section.

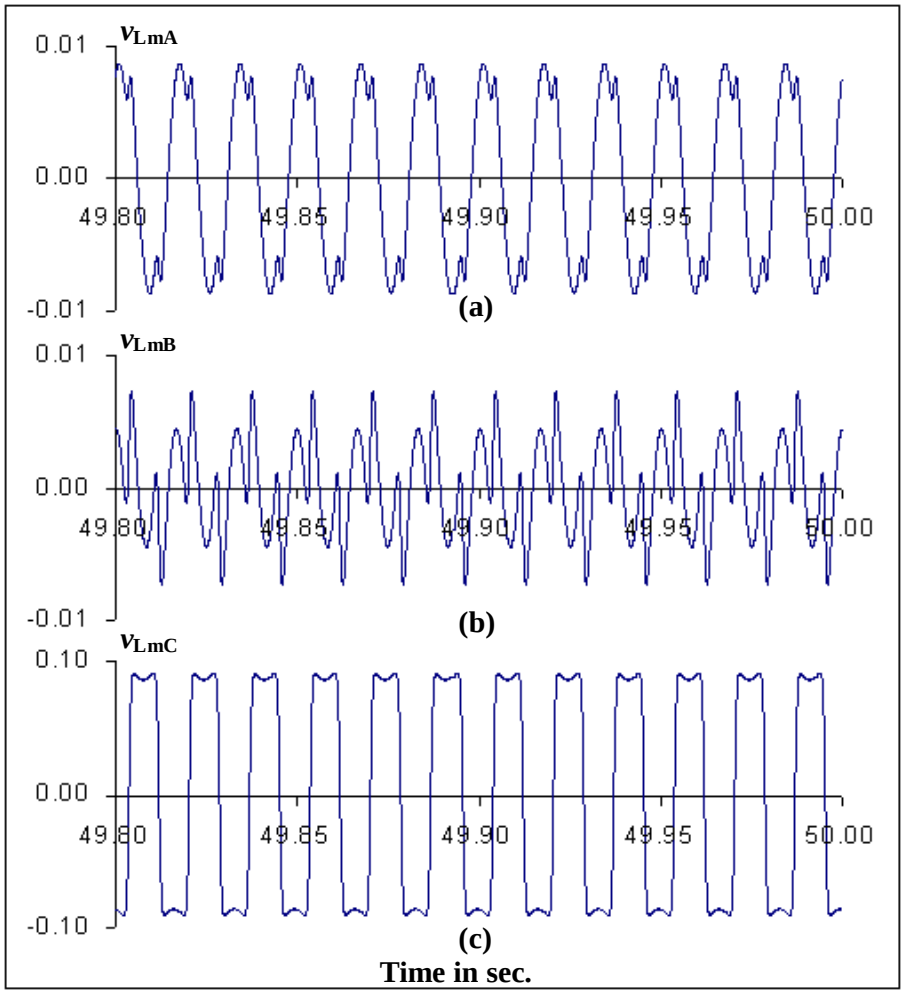

Fig.6.36 Time plots of fundamental solution, I_{Np} = 1.0 A, q = 11, linear core loss, C_g = 100% of base case value.

(a) Phase A transformer voltage.
(b) Phase B transformer voltage.
(c) Phase C transformer voltage.

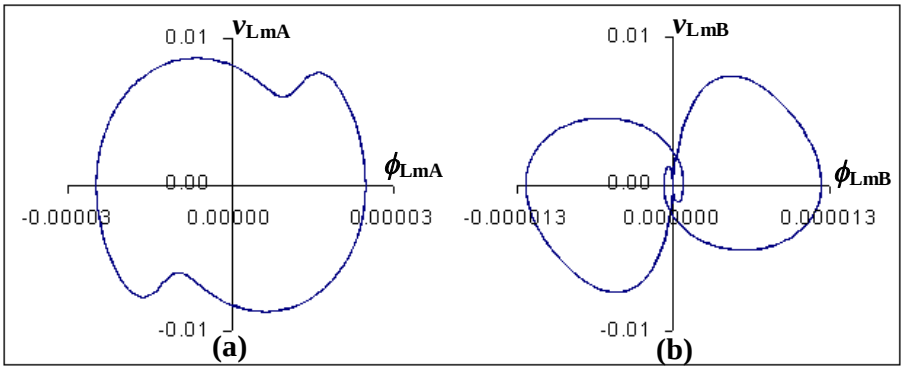

Fig.6.37 Phase plots of fundamental solution.

(a) Phase plot of Fig.6.36a.
(b) Phase plot of Fig.6.36b.

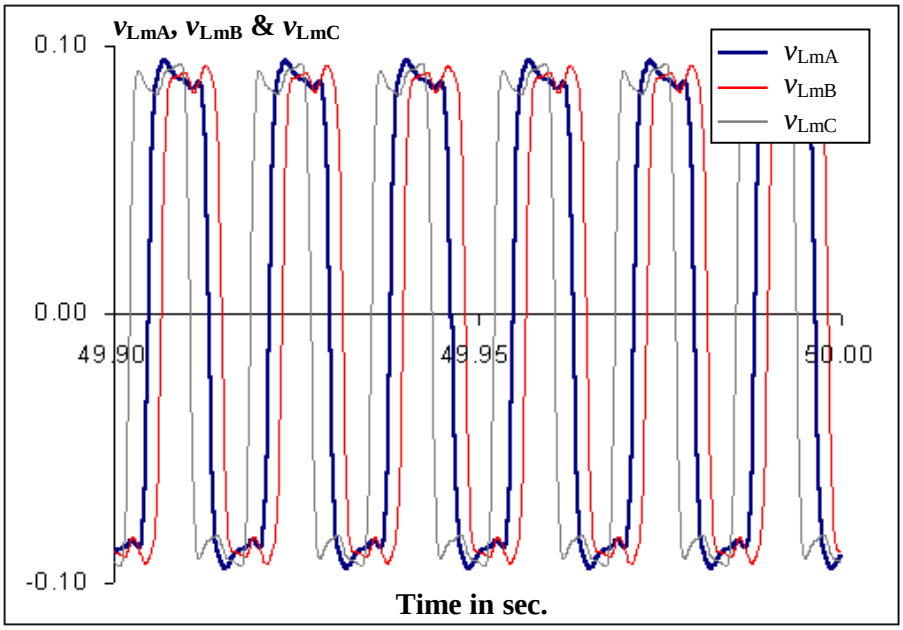

Fig.6.38a Time plots of fundamental solution, I_{Np} = 2.0 A, q = 11, linear core loss, C_g = 100% of base case value.

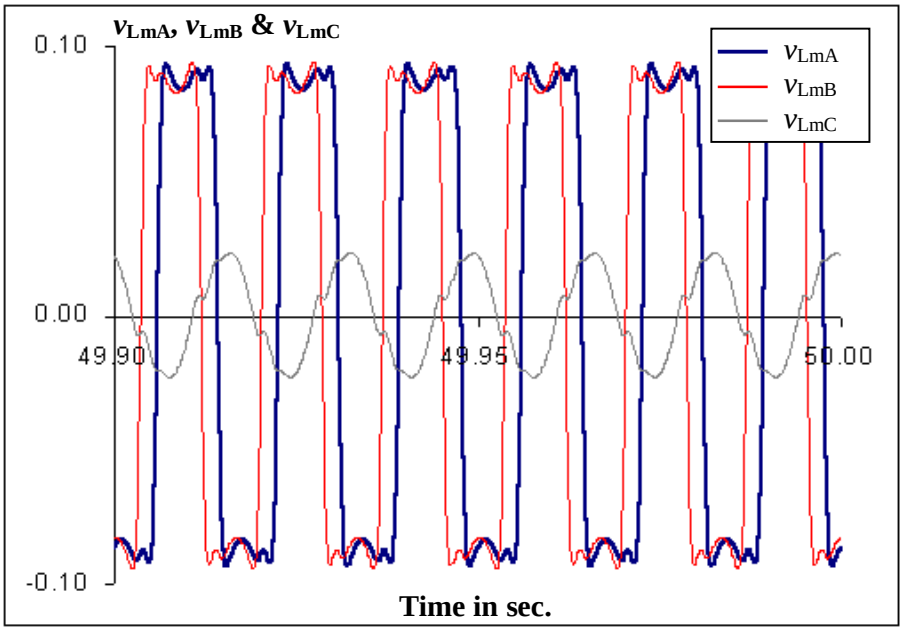

Fig.6.38b Time plots of fundamental solution, I_{Np} = 3.0 A, q = 11, linear core loss, C_g = 100% of base case value.

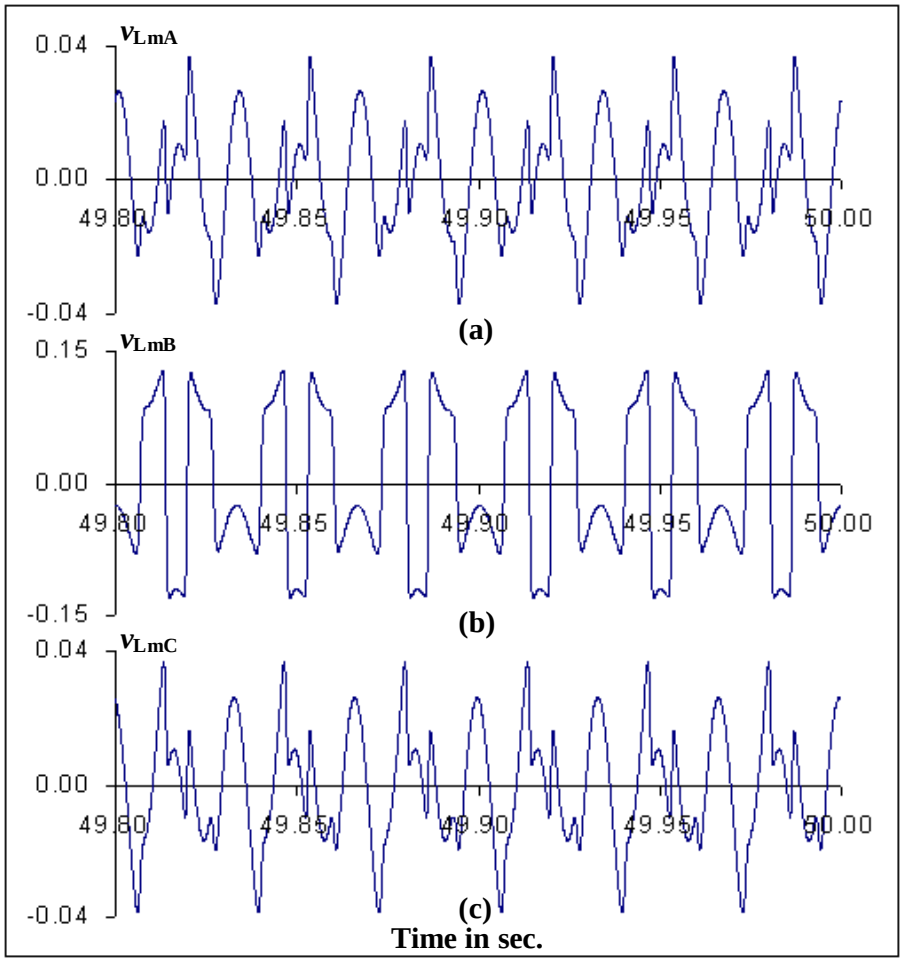

Fig.6.39 Time plots of period 2 solution, I_{Np} = 1.49 A, q = 11, linear core loss, C_g = 100% of base case value.

(a) Phase A transformer voltage.
(b) Phase B transformer voltage.
(c) Phase C transformer voltage.

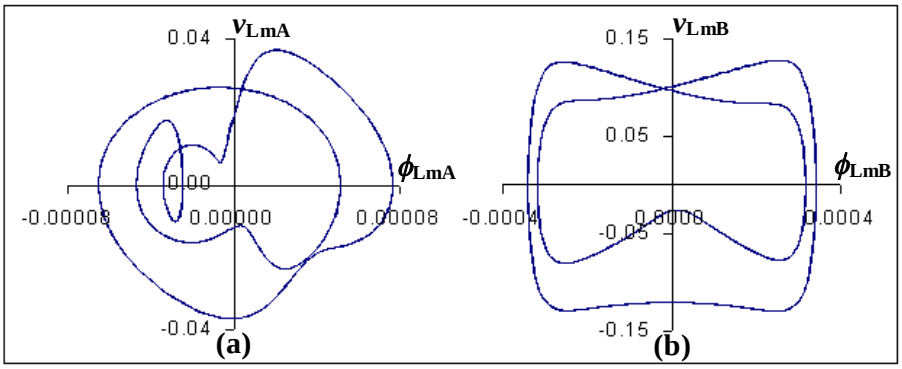

Fig.6.40 Phase plots of period 2 solution.

(a) Phase plot of Fig.6.39a.
(b) Phase plot of Fig.6.39b.

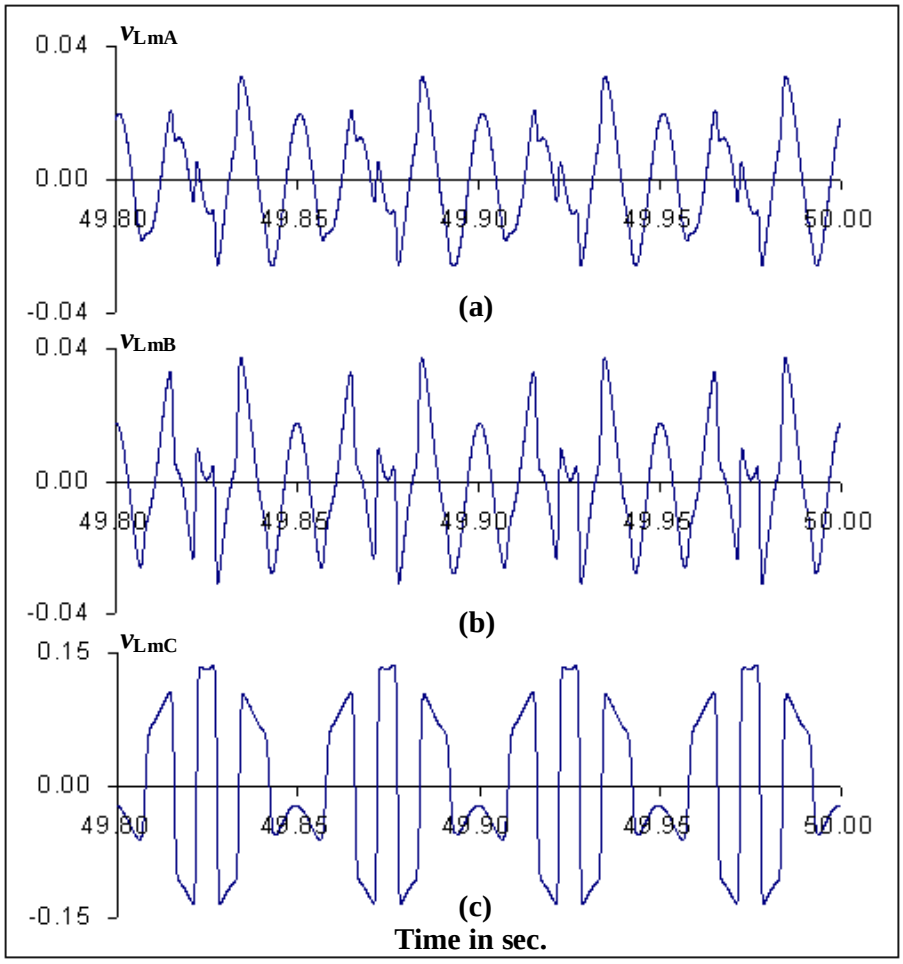

Fig.6.41 Time plots of period 3 solution, I_{Np} = 0.93 A, q = 11, linear core loss, C_g = 100% of base case value.

(a) Phase A transformer voltage.
(b) Phase B transformer voltage.
(c) Phase C transformer voltage.

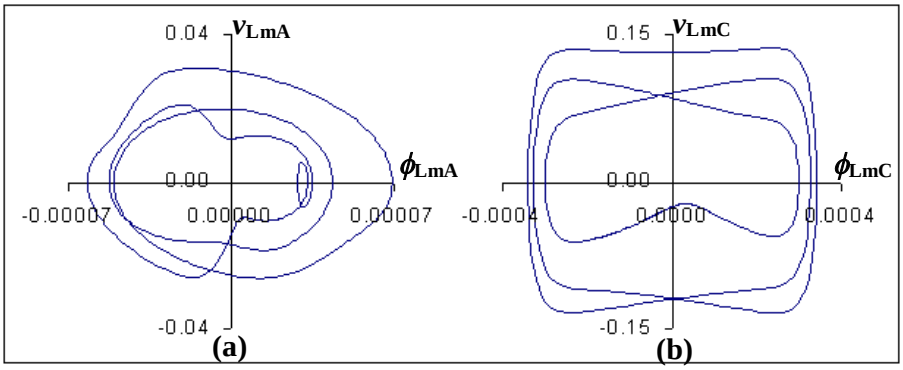

Fig.6.42 Phase plots of period 3 solution.

(a) Phase plot of Fig.6.41a.
(b) Phase plot of Fig.6.41c.

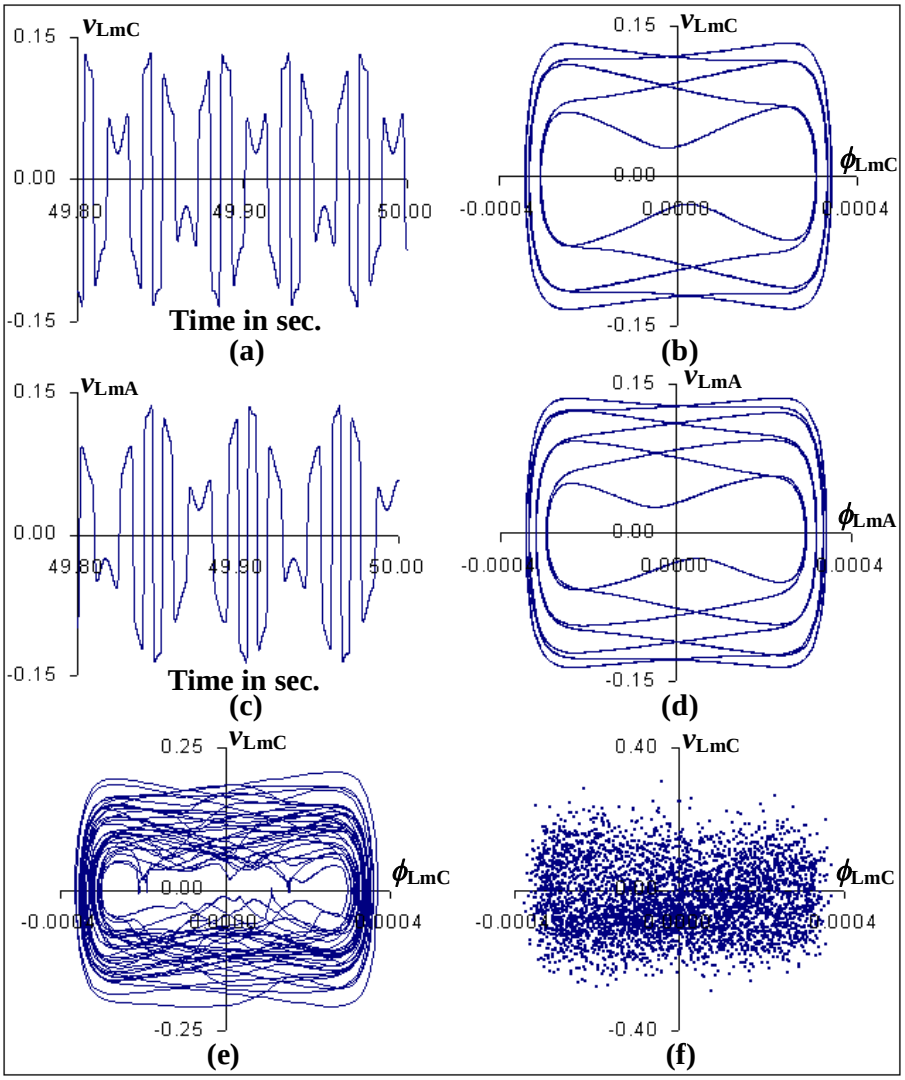

Fig.6.43 Time, phase plots and conventional Poincaré map, q = 11, linear core loss model, C_g = 100% of base case value.

(a) Time plots of P_5 solution, I_{Np} = 1.13 A, phase C voltage.
(b) Phase plot of Fig.6.43a.
(c) Time plots of P_5 solution, I_{Np} = 0.75 A, phase A voltage.
(d) Phase plot of Fig.6.43c.
(e) Phase plot of chaotic solution, I_{Np} = 2.50 A, phase C.
(f) Conventional Poincaré map of Fig.6.43e.

6.5.2 Bifurcation diagram of steady state isolated subharmonic solutions

Figures 6.44 and 6.45 show the bifurcation diagram of different period 2 solutions. The initial period 2 steady states are obtained from temporal bifurcation diagram, Fig.6.35b. Time domain and phase plots of different period 2 and period 4 (due to period doubling) oscillations are shown in Figures 6.46 and 6.47. The time domain and phase plots in Fig.6.46 correspond to the different stable and unstable period 2 solutions in Fig.6.44. Plots shown in Fig.6.47 correspond to the different stable and unstable period 2 solutions in Fig.6.45. It can be seen that the solutions are skew-symmetric.

The continua of different period 3 solutions are shown in Fig.6.48 and Fig.6.49. Supercritical and subcritical pitchfork bifurcations are identified in period 3 solution paths. The point PF in Fig.6.48 is a supercritical pitchfork bifurcation point. The stable symmetric period 3 branch (s-a) degenerates to two stable non symmetric period 3 branches (a-b, a-c), each of which is followed by a flip segment. Fig.6.50 shows the magnified view of box A in Fig.6.49. It confirms the existence of multiple stable period 3 solutions (P_{3a} to P_{3d} in figure). The magnified view of box B in Fig.6.50 is shown in Fig.6.51. The point PF in Fig.6.51 is a subcritical pitchfork bifurcation point, where an unstable periodic branch (s-a) loses its stability and a stable branch (a-d) along with two unstable branches (a-b, a-c) appear. The upward and downward arrows in the figure indicate the culmination of unstable solutions into stable solutions in their vicinity. Figure 6.52 and 6.53 show the time and phase plots of symmetric and non symmetric period 3 solutions of Fig.6.48. The time plots of different period 3 solutions around $I_{Np} = 0.7$ A of Fig.6.50 are shown in Figures 6.54 and 6.55.

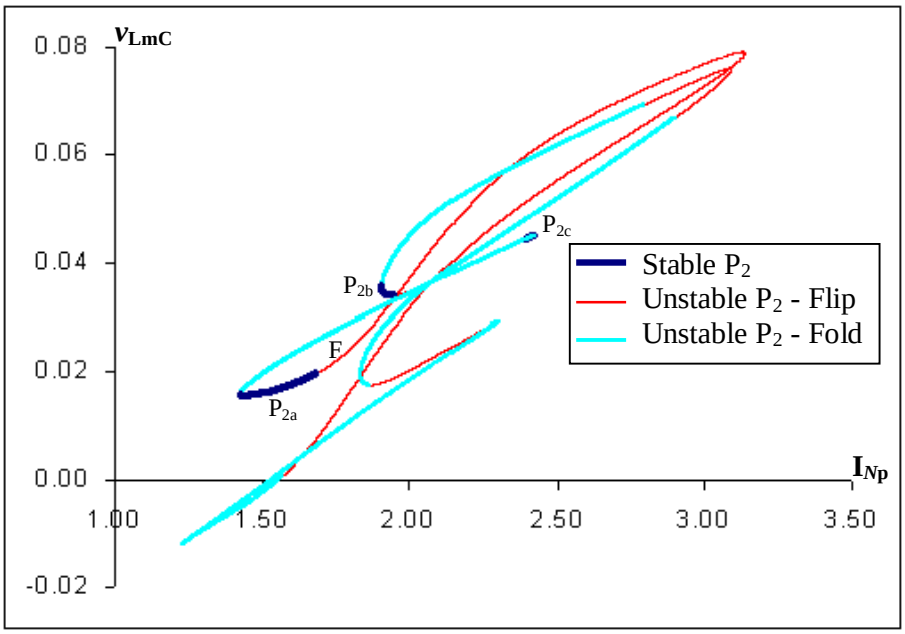

Fig.6.44 Bifurcation diagram of steady state period 2 solution, q = 11, linear core loss model, C_g = 100% of base case value. P_{2a} to P_{2c} - different period 2 solution segments. The initial steady state is obtained from temporal bifurcation diagram, Fig.6.35b.

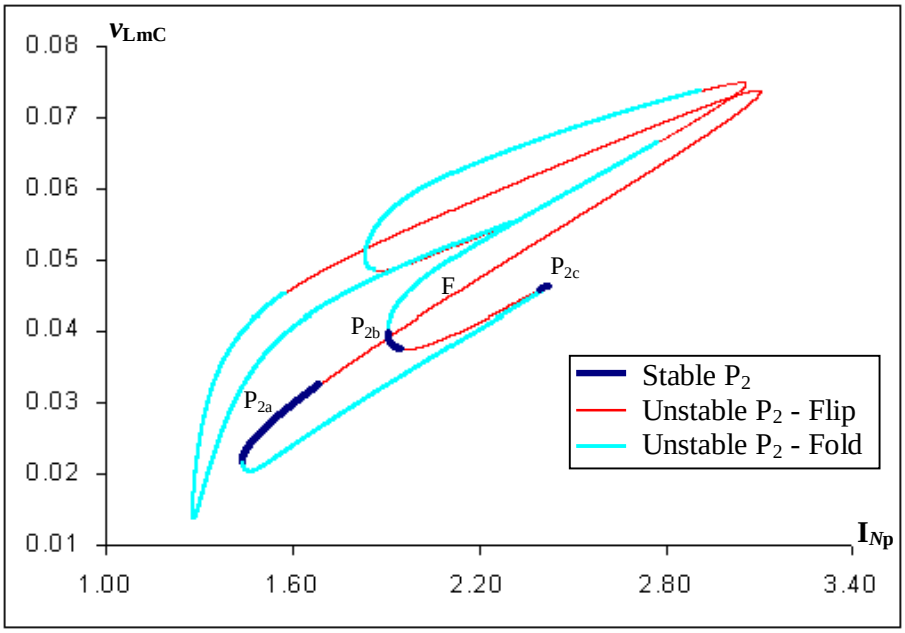

Fig.6.45 Bifurcation diagram of steady state period 2 solution, q = 11, linear core loss model, C_g = 100% of base case value. P_{2a} to P_{2c} - different period 2 solution segments. The initial steady state is obtained from temporal bifurcation diagram, Fig.6.35b.

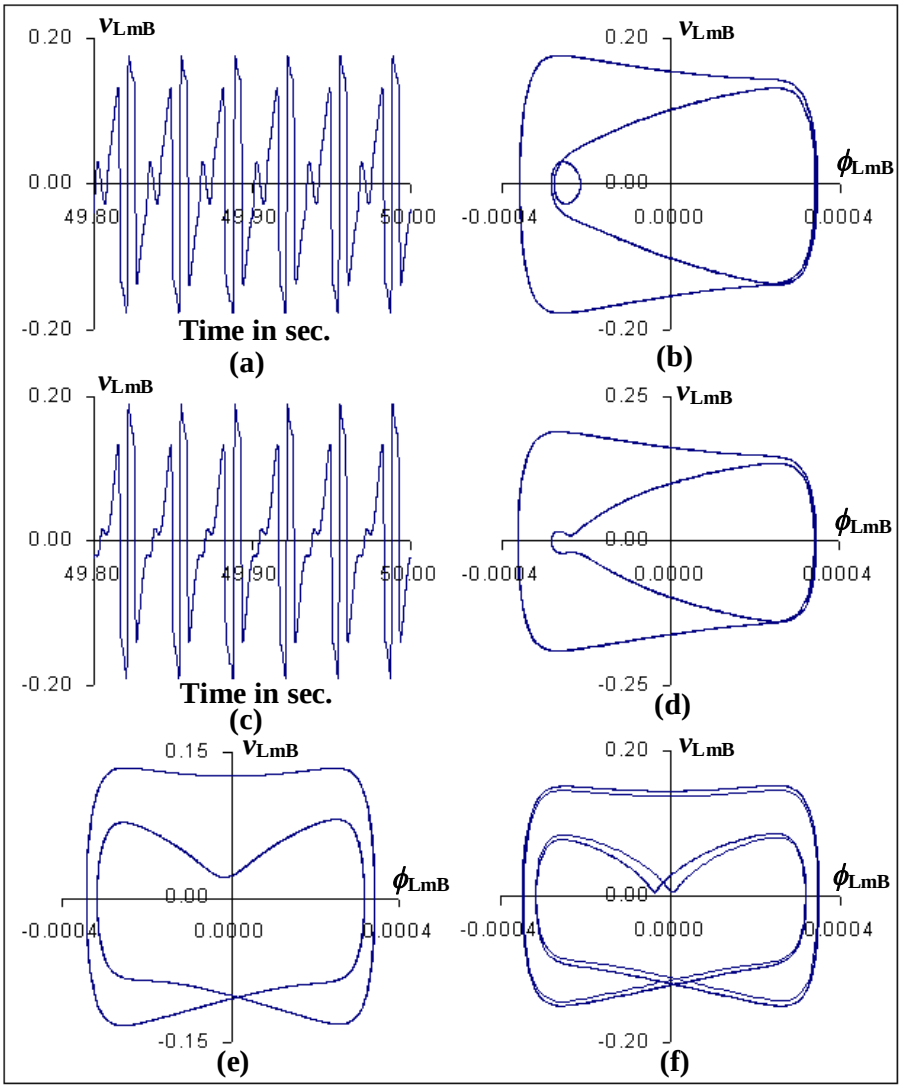

Fig.6.46 Time domain and phase plots of phase B period 2 oscillations, q = 11, linear core loss model, C_g = 100% of base case value.

(a) Time plot of P_2 solution at I_{Np} = 1.95 A (in P_{2b} of Fig.6.44)
(b) Phase plot of Fig.6.46a.
(c) Time plot of P_2 solution at I_{Np} = 2.40 A (in P_{2c} of Fig.6.44)
(d) Phase plot of Fig.6.46c.
(e) Phase plot of P_2 solution at I_{Np} = 1.52 A (in P_{2a} of Fig.6.44)
(f) Phase plot of P_4 solution at I_{Np} = 1.70 A (in F of Fig.6.44)

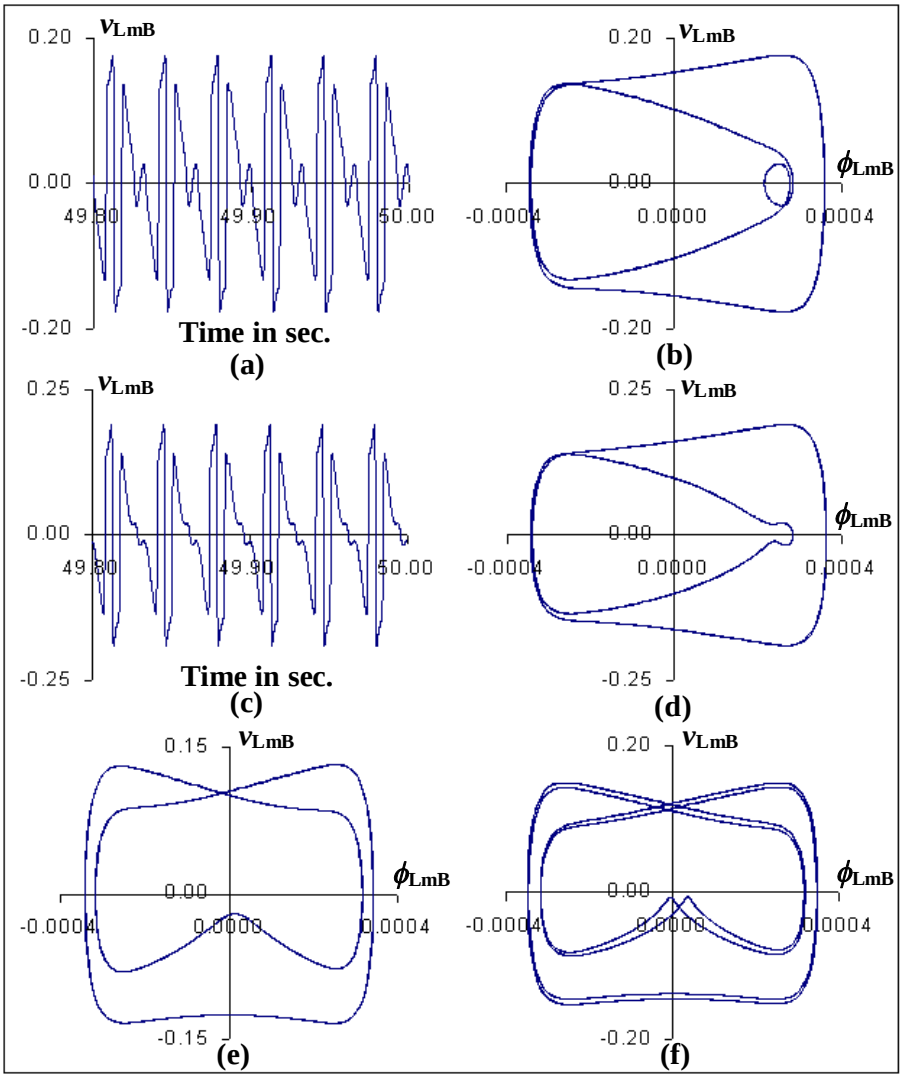

Fig.6.47 Time domain and phase plots of phase B period 2 oscillations, q = 11, linear core loss model, C_g = 100% of base case value.

(a) Time plot of P_2 solution at I_{Np} = 1.95 A (in P_{2b} of Fig.6.45)
(b) Phase plot of Fig.6.46a.
(c) Time plot of P_2 solution at I_{Np} = 2.40 A (in P_{2c} of Fig.6.45)
(d) Phase plot of Fig.6.46c.
(e) Phase plot of P_2 solution at I_{Np} = 1.52 A (in P_{2a} of Fig.6.45)
(f) Phase plot of P_4 solution at I_{Np} = 1.70 A (in F of Fig.6.45)

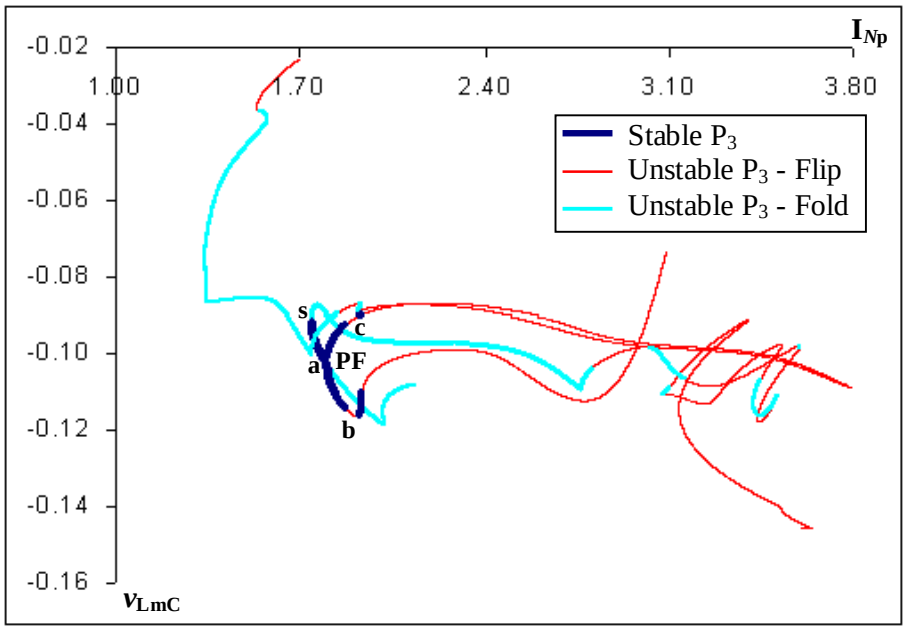

Fig.6.48 Bifurcation diagram of steady state period 3 solution, q = 11, linear core loss model, C_g = 100% of base case value. PF – supercritical pitchfork bifurcation point. The initial steady state is obtained from temporal bifurcation diagram, Fig.6.35b.

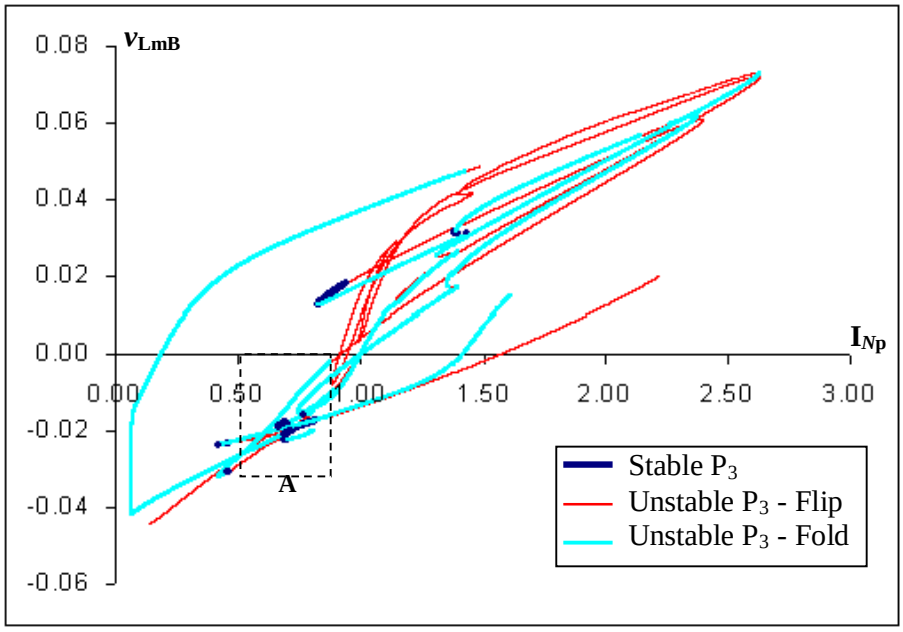

Fig.6.49 Bifurcation diagram of steady state period 3 solution, q = 11, linear core loss model, C_g = 100% of base case value. The initial steady state is obtained from temporal bifurcation diagram, Fig.6.35b.

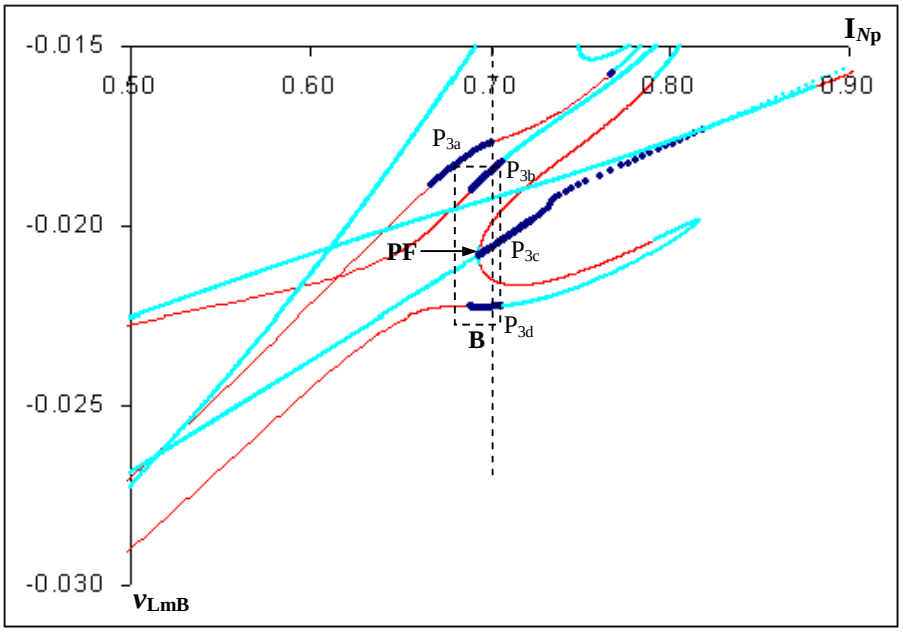

Fig.6.50 Magnified view of box A of Fig.6.49. PF – subcritical pitchfork bifurcation point.

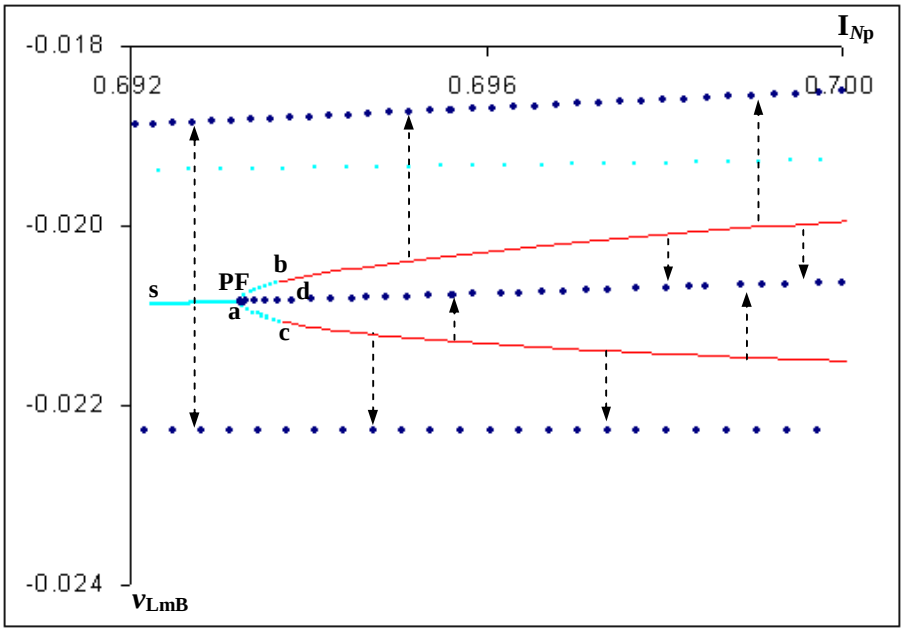

Fig.6.51 Magnified view of box B of Fig.6.50. PF – subcritical pitchfork bifurcation point.

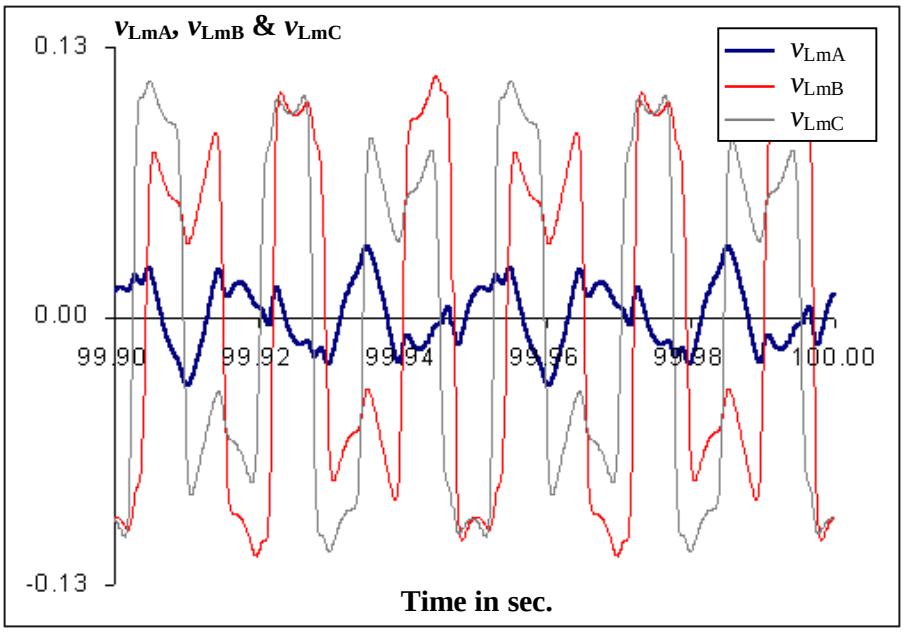

Fig.6.52 Time domain plot of symmetric period 3 solution at I_{Np} = 1.77 A of Fig.6.48.

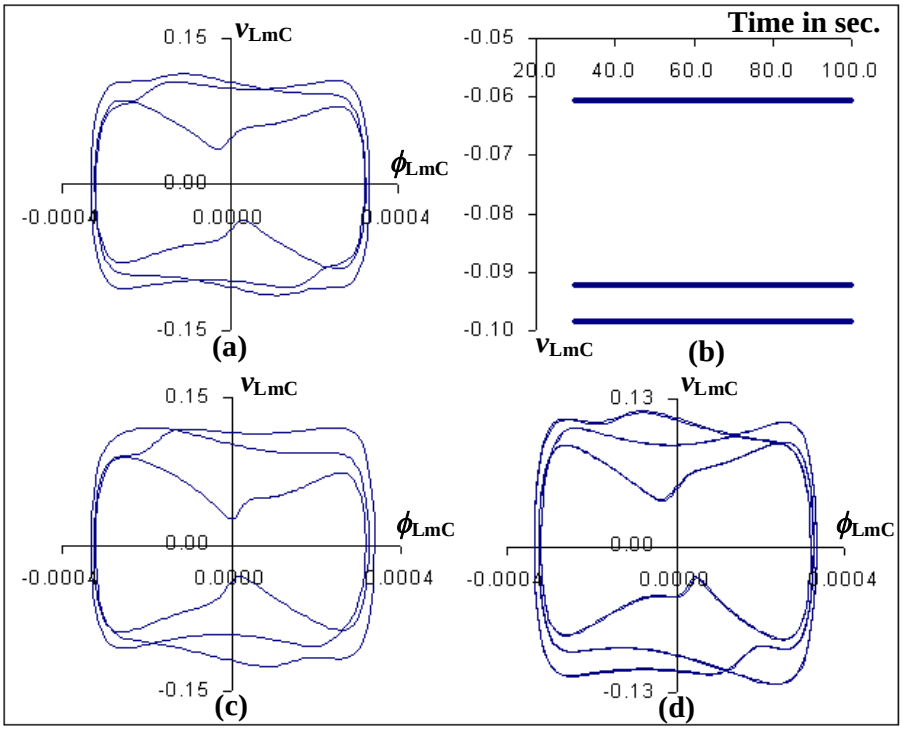

Fig.6.53 Phase plots of period 3 and period 6 oscillations of Fig.6.48.

(a) Phase plot corresponding to phase C voltage of Fig.6.52.
(b) Evolving Poincaré map of Fig.6.53a.
(c) Phase plot of non symmetric P_3 solution at I_{Np} = 1.869 A.
(d) Phase plot of P_6 solution at I_{Np} = 1.936 A.

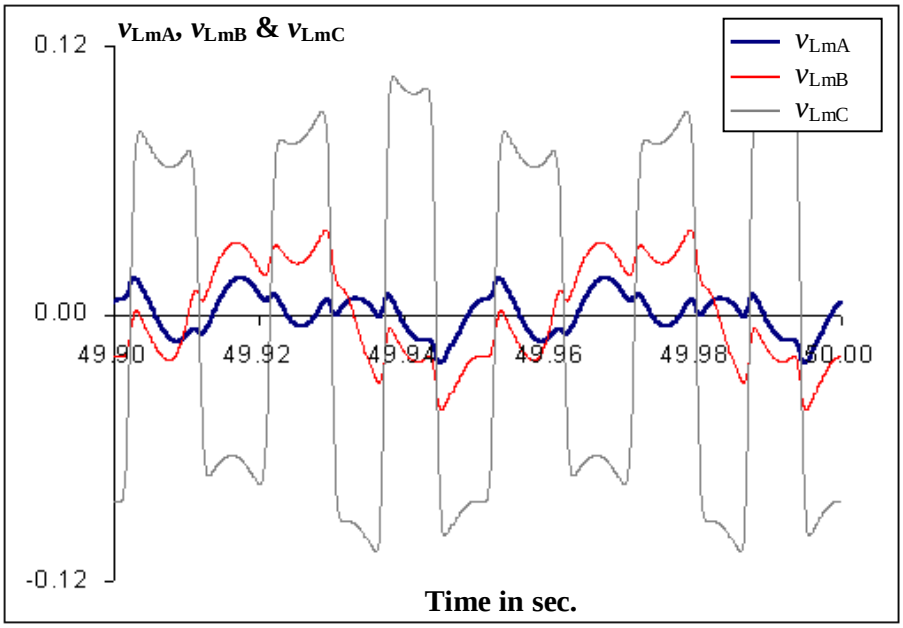

Fig.6.54 Time domain plot of period 3 solution at I_{Np} = 0.70 A in segment P_{3b} of Fig.6.50.

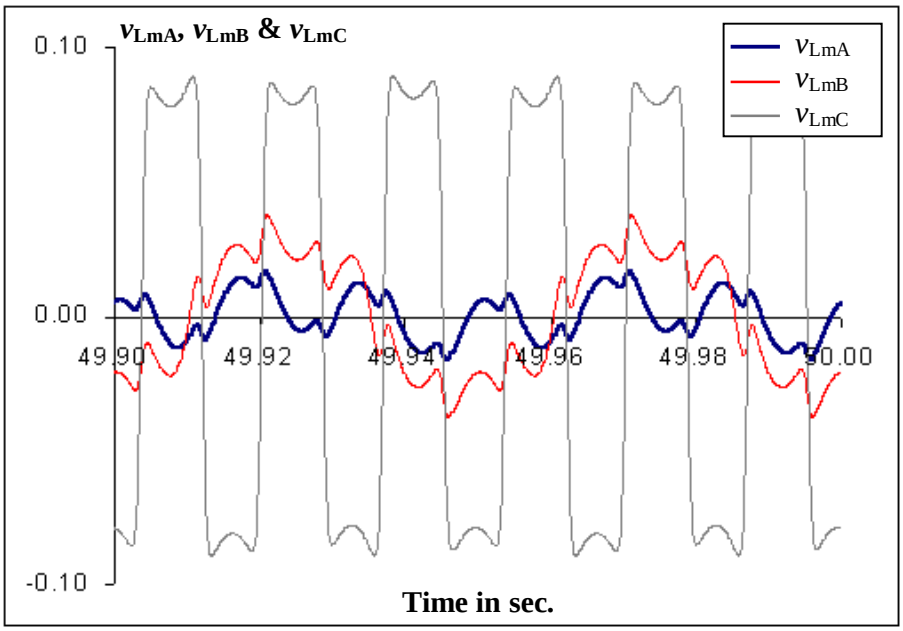

Fig.6.55 Time domain plot of period 3 solution at I_{Np} = 0.70 A in segment P_{3c} of Fig.6.50.

The continuum of period 5 and period 7 solutions are shown in Fig.6.56 and Fig.6.57, for which the initial steady states are obtained from temporal bifurcation diagram, Fig.6.35b. The corresponding time domain plots of period 5 and period 7 solutions are given in Figures 6.58 and 6.59.

Figures 6.60 and 6.61 depict the continuum of period 2 and period 3 solutions corresponding to higher capacitance to ground cases. The initial steady states are obtained from temporal bifurcation diagram, Fig.6.35d. It can be seen from the Figures 6.60 and 6.45 that subharmonic solutions occur for wider range of bifurcation parameter. Further, they commence at a higher value of bifurcation parameter. Figures 6.61 and 6.49 also confirm the same. The time plots of different period 3 solutions in Fig.6.60 are shown in Figures 6.62 and 6.63.

The continuum of period 5 and period 7 solutions shown in Figures 6.64 and 6.65 also confirm the occurrence of subharmonic solutions for wider range of parameter for higher capacitance to ground. The time plots of period 5 and period 7 solutions are given in Fig.6.66 and Fig.6.67.

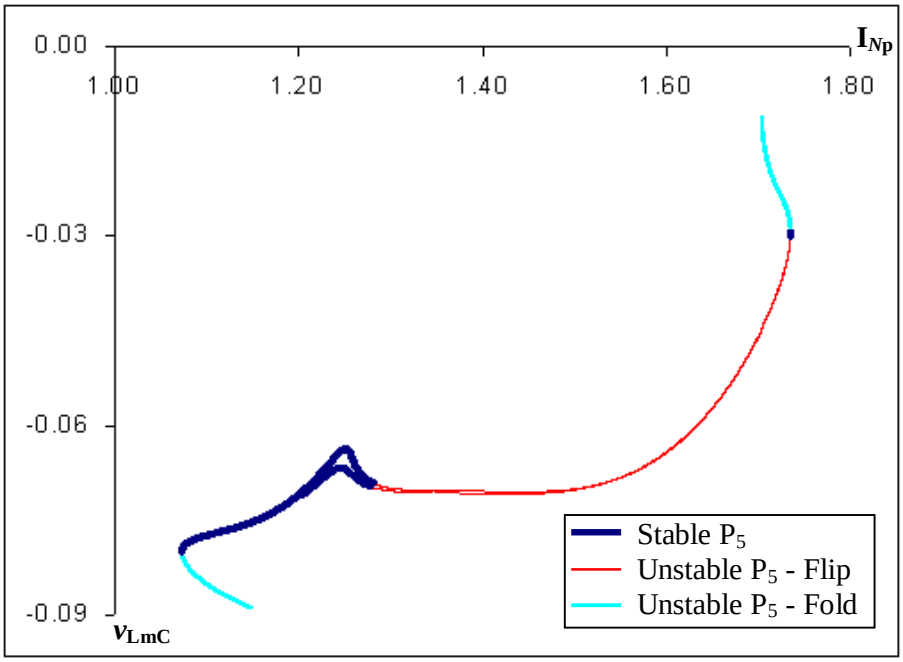

Fig.6.56 Bifurcation diagram of steady state period 5 solution, q = 11, linear core loss model, C_g = 100% of base case value. The initial steady state is obtained from temporal bifurcation diagram, Fig.6.35b.

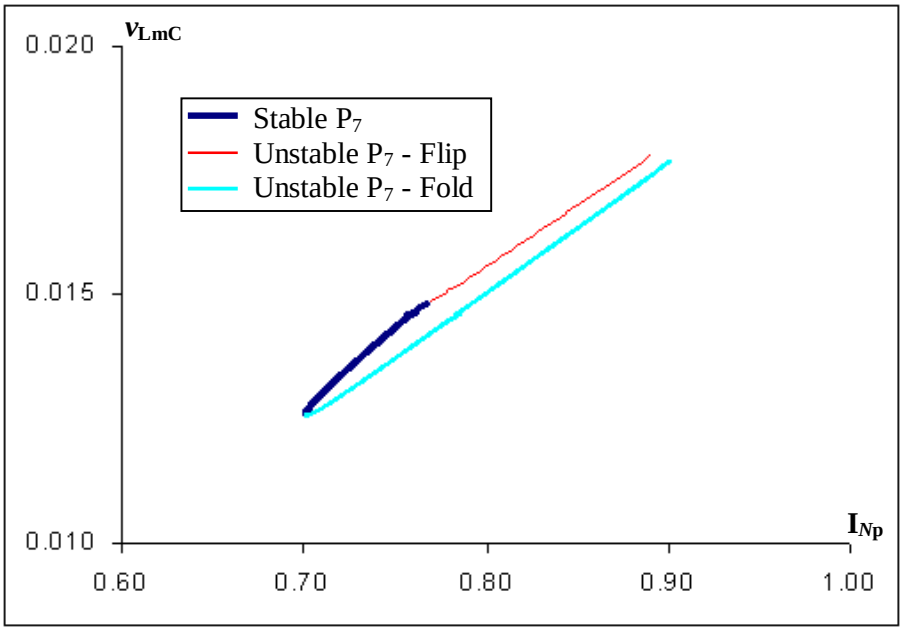

Fig.6.57 Bifurcation diagram of steady state period 7 solution, q = 11, linear core loss model, C_g = 100% of base case value. The initial steady state is obtained from temporal bifurcation diagram, Fig.6.35b.

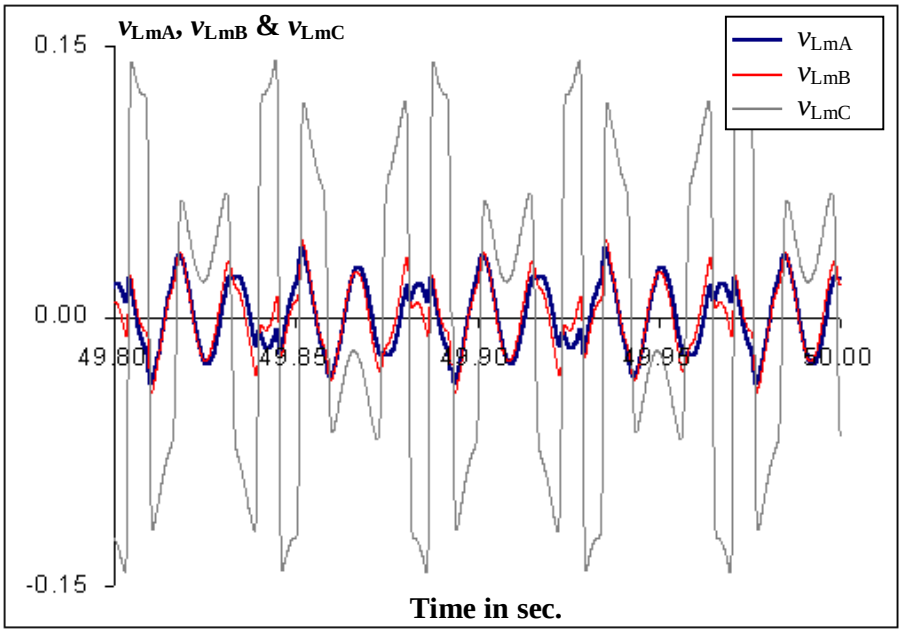

Fig.6.58 Time domain plot of period 5 solution at I_{Np} = 1.21 A in Fig.6.56.

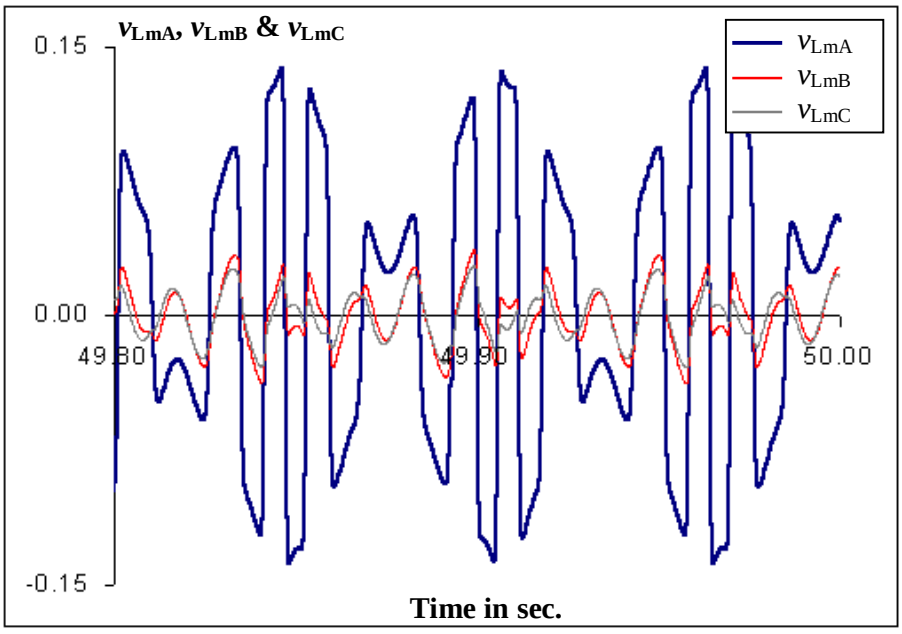

Fig.6.59 Time domain plot of period 7 solution at I_{Np} = 0.764 A in Fig.6.57.

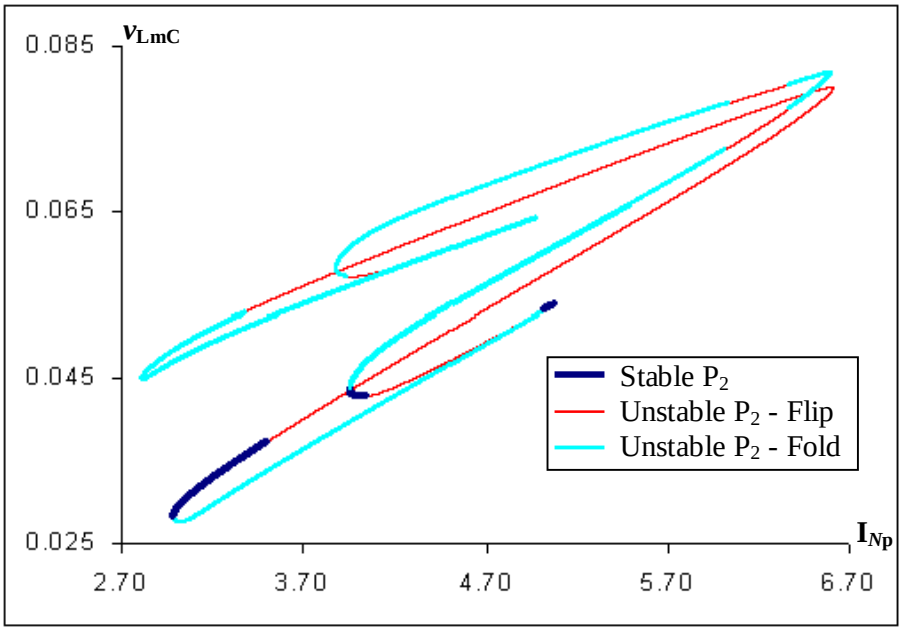

Fig.6.60 Bifurcation diagram of steady state period 2 solution, q = 11, linear core loss model, C_g = 200% of base case value. The initial steady state is obtained from temporal bifurcation diagram, Fig.6.35d.

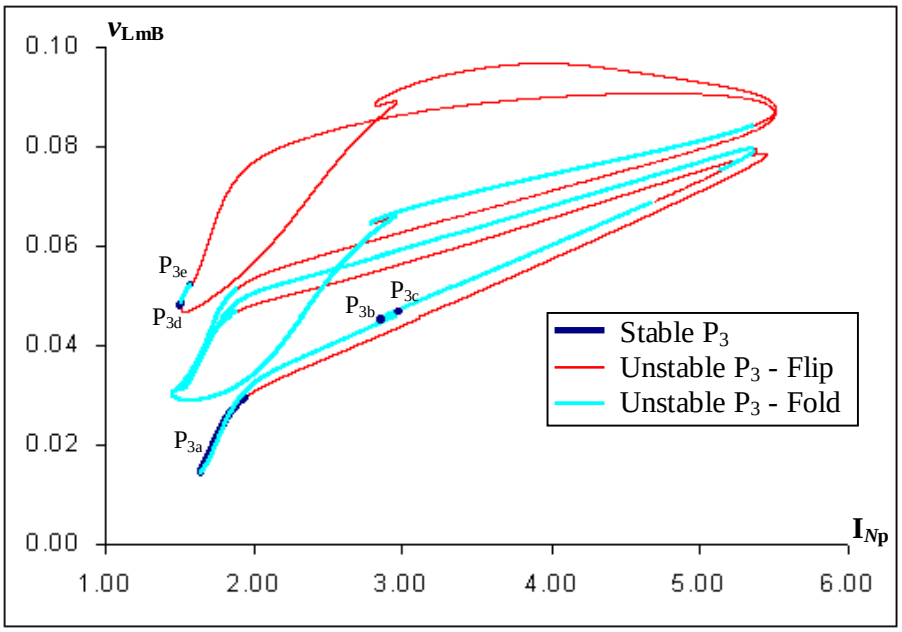

Fig.6.61 Bifurcation diagram of steady state period 3 solution, q = 11, linear core loss model, C_g = 200% of base case value. P_{3a} to P_{3e} - different period 3 solution segments. The initial steady state is obtained from temporal bifurcation diagram, Fig.6.35d.

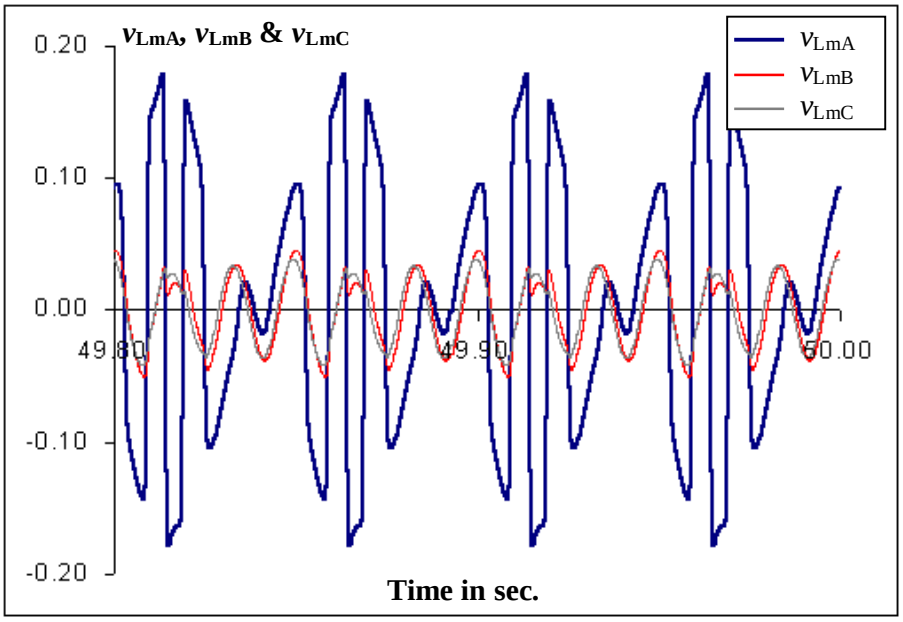

Fig.6.62 Time domain plot of period 3 solution at I_{Np} = 2.856 A in segment P_{3b} of Fig.6.61.

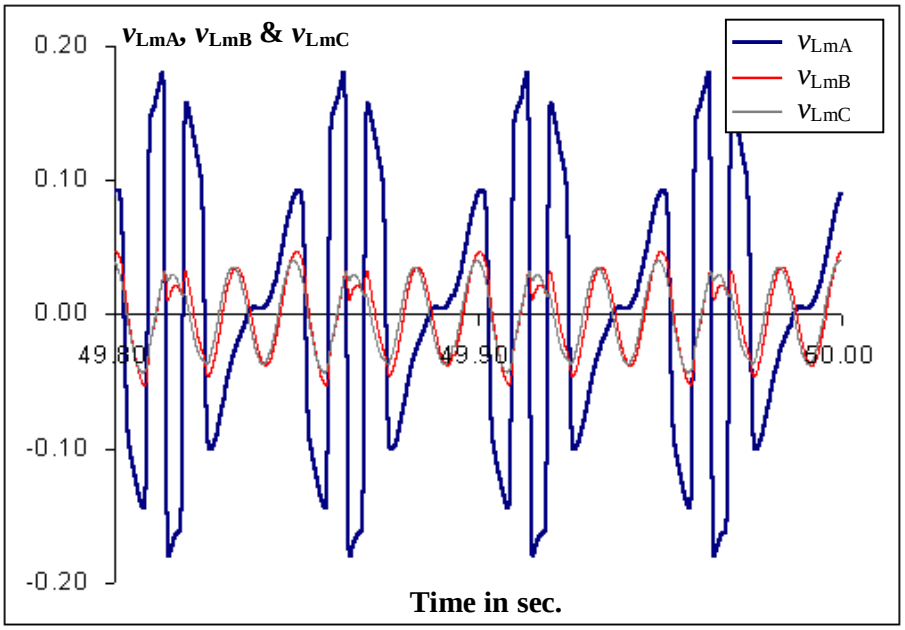

Fig.6.63 Time domain plot of period 3 solution at I_{Np} = 2.986 A in segment P_{3c} of Fig.6.61.

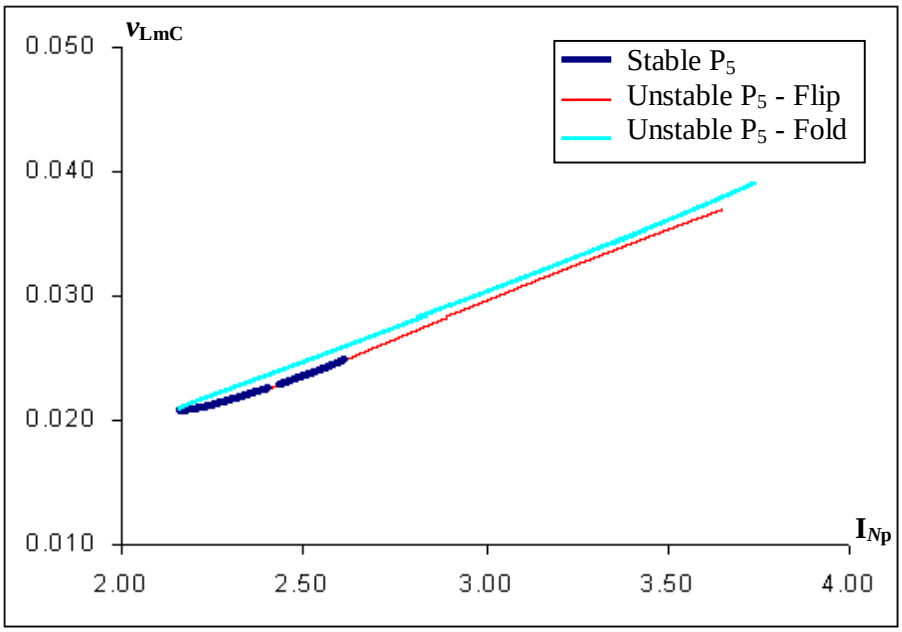

Fig.6.64 Bifurcation diagram of steady state period 5 solution, q = 11, linear core loss model, C_g = 200% of base case value. The initial steady state is obtained from temporal bifurcation diagram, Fig.6.35b.

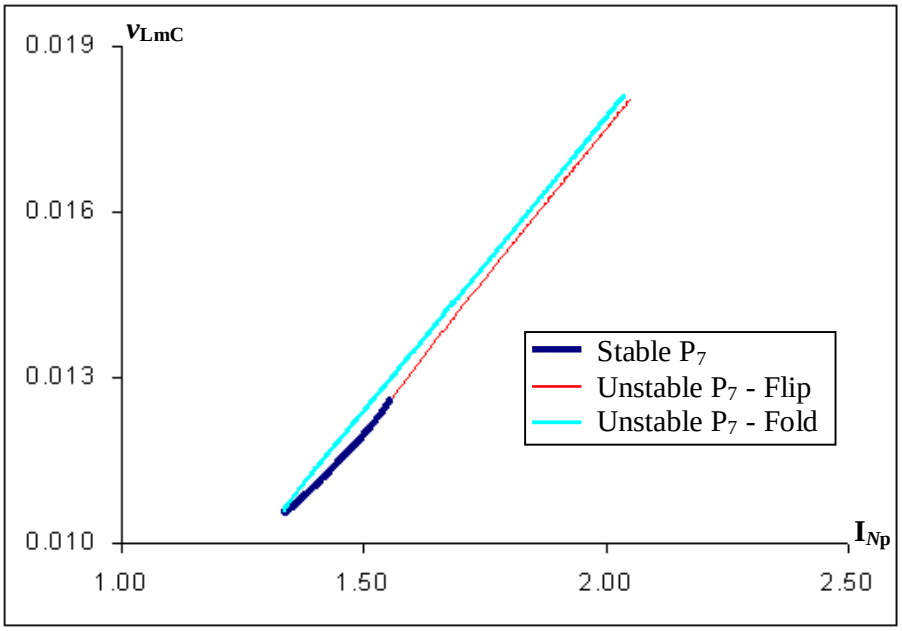

Fig.6.65 Bifurcation diagram of steady state period 7 solution, q = 11, linear core loss model, C_g = 200% of base case value. The initial steady state is obtained from temporal bifurcation diagram, Fig.6.35d.

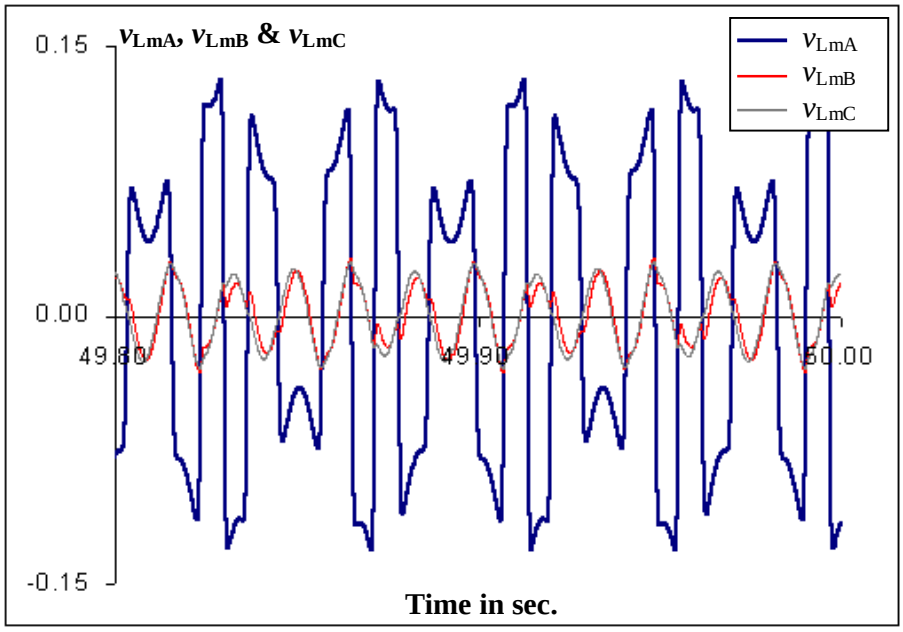

Fig.6.66 Time domain plot of period 5 solution at I_{Np} = 2.247 A of Fig.6.64.

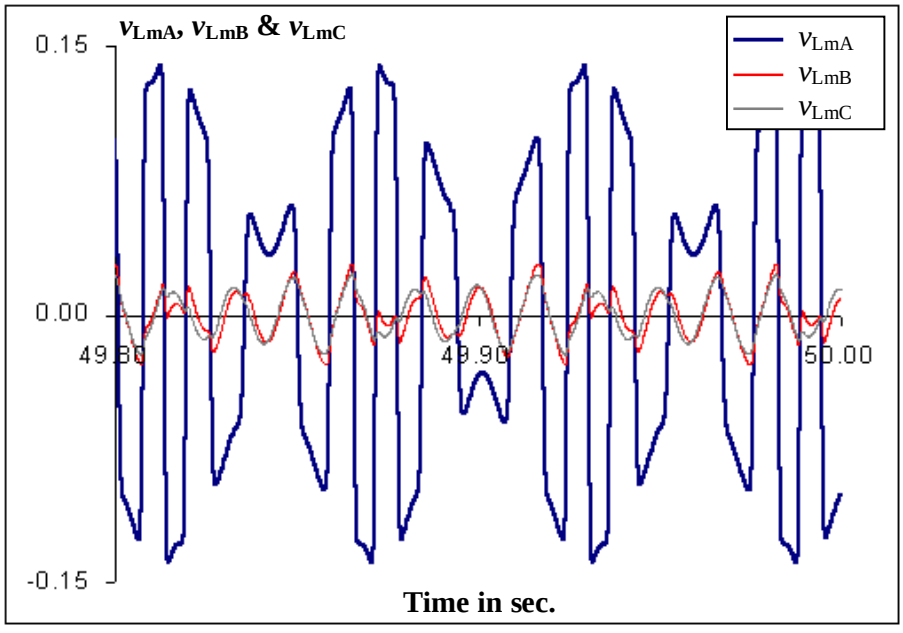

Fig.6.67 Time domain plot of period 7 solution at I_{Np} = 1.45 A of Fig.6.65.

6.6 SUMMARY

Extensive simulations have been carried out to assess the isolated subharmonic behaviour of the practical power systems. The 1100 kV system of BPA has been used for the analysis of the effect of core loss nonlinearity on isolated subharmonics. The sensitivity of isolated subharmonics with respect to length of de-energised line has been analysed for the 525 kV system of BPA.

Analysis reveals the following:
Conclusions obtained for the 1100 kV system:

- Increase in saturation index is accompanied by the onset of subharmonics for lower values of parameter.
- Existence of stable subharmonic solutions decreases with increase in core saturation.
- Number of bifurcation points increases with increase in core saturation.
- The inclusion of nonlinearity in core loss results in

    i) Solutions that are more optimistic when compared with linear models.
    ii) Elimination of nearly all subharmonic oscillations for the range of parameter considered.

- Most of the symmetric odd subharmonic solutions undergo supercritical pitchfork bifurcation.
- In most cases, supercritical pitchfork bifurcation is followed by period doubling bifurcation.

Conclusions obtained for the 525 kV system:

- Higher core saturation index increases the possibility of chaotic ferroresonance for practical values of parameter.
- Higher capacitance to ground of the de-energised line widens the range of subharmonic solutions. Further, subharmonic solutions commence at a higher value of parameter.
- Onset of chaos occurs at a higher value of parameter for higher capacitances.
- Supercritical and subcritical pitchfork bifurcations are likely to occur in odd subharmonic solution paths.